ASSESSMENT OF GLIOMA RESPONSE TO 8 GY RADIOTHERAPY ON MULTIPLE MRI BIOMARKERS BY APPLYING IMAGE SEGMENTATION ALGORITHM

By

Yang Yu

A thesis submitted to Johns Hopkins University in conformity with the requirements for the degree of Master of Science

Baltimore, Maryland

May, 2015

ABSTRACT

Magnetic Resonance Imaging (MRI) is playing a significant role in assessment of treatment response for a variety of diseases. To investigate multi-parametric MRI biomarkers for the assessment of glioma response to radiotherapy, we made comparison among different MRI parameters. In the tumor extraction step, we compare the manual segmentation, automatic and semi-automatic methods based on region of interest (ROI) results. In our experiments, thirteen nude rats injected with U87 tumor were irradiated by 8 Gy radiation dose. All MRI were performed on a 4.7 T animal scanner at time points of pre-radiation, 1 day, 4 days and 8 days post-radiation. Multi-parametric MRI signals of the tumors were compared in quantitative. Two experts performed manual and semi-automatic methods on tumor extraction on Amide Proton Transfer-weighted (APTw) maps.

The results shows that average Apparent Diffusion Coefficient (ADC) intensity of ROI had a great increase during the post-radiation. The relative blood flow values (tumor vs. normal contralateral side of brain) had a continuous decrease after radiotherapy. Similarly, APTw signals intensity decreased at all time after radiotherapy. Semi-automatic method gave a more stable ROI extraction result on APTw maps than manual segmentation without rater dependence, and with less time consumption.

In conclusion, ADC, blood flow, APTw are all helpful signals in assessing glioma response to radiotherapy. Also, semi-automatic method on ROI extraction showed higher efficiency and stability than manual method.

Advisor: Jinyuan Zhou, Ph.D. Readers: Ye Qiao, Ph.D. and Kevin Yarema, Ph.D.

ACKNOWLEDGEMENTS

During the past two years of my way to master, the important lesson that I learn here is that research requires time and efforts. Although the research is not easy or straightforward, my advisor Dr. Jinyuan Zhou patiently answered all my questions or doubt that I may have, and gave me some advise that lets me explore new field with brainstorm and new ideas.

I would like to also thank so many individuals who have support me and give me instruction to this work and my progress. Members in Dr. Zhou's lab have trained me numerous techniques and always given me suggestions on algorithms improvements and statistics analysis during each group meeting. Dr. Shin-Lei Peng offered me some instructions about the data analysis and related knowledge. The study did not always go as planned, while she and other members in my lab support me and their continued guidance encourages me. Dr. Kai Zhang acted as second rater in my experiment, giving me the chance to make comparison between different methods. Dr. Haiyun Li provided me some advice on image segmentation algorithm and broadened my horizon in related field.

On all the way of my life in Johns Hopkins University, I appreciate my family and friends' encouragements. They stay along with me by heart during these two years, although they are not physically beside me. My soul mate, Wan Su, is the girl that I cannot thank enough for her persistent support and the help she supplied me for the past few weeks. Last, but never the least, my parents and aunt have always offered their unconditional support, and I would not be where I am without their loving assistance. They are my constant inspiration and derivation of feeling blessed and grateful, for their spirit guidance as always.

CONTENTS

LIST OF FIGURES

1. Introduction

1.1 Gliomas

Among the new cases of malignant primary brain tumors, gliomas account for 5 to 10 per 100,000 individuals worldwide, which is the most common type that has been identified, with the median survival 12 to 15 months for patients[1, 2]. The cell of the origin of primary brain tumor is still unknown, however, we have assured that according to histology analysis, this kind of tumors are similar with astrocytes, oligodendrocytes or ependymoma. In 2007, World Health Organization (WHO) announced that based on histology, gliomas were classified into four grades from I to IV. Grade I and II are low-grade gliomas levels, with better prognosis and treatment outcome. The Grade III and IV considered high-grade gliomas levels, are relative fast-growing, undifferentiated and usually have a worse prognosis. Approximately 60% cases of glioblastomas are diagnosed as high-grade gliomas. Grade III tumors has two to three years survival rate in median and around one year for those with grade IV tumors. The glioblastomas are diagnosed at all ages while senior patients with higher-grade gliomas have shorter survival for the poor performance status. Depends on the size, position and the degree of infiltration of the gliomas, brain tumors have variable presentation, such as seizures, headaches, speech, sensory or motor symptoms[3].

Current treatments such as chemotherapy following the surgery, has been proved to improve survival over surgery alone while the optimal chemotherapeutic regimen alone for glioblastoma is not suggested at present. Considered as an adjuvant treatment method, chemotherapy combines the procarbazine, lomustine and vincristine, or single-agent treatment

with carmustine or lomustine as frequent used regimens[4]. Photodynamic therapy is a novel treatments way involves using a laser to target lesions after rendering them light-sensitive. The evidence of efficacy is being evaluated by the National Institute for Health and Clinical Excellence (NICE)[5]. In 1970s, Walker carried a research and radiation therapy had been proposed to be an effective method in diagnosed malignant glioma (MG) treatments which can prolong patients' survival[4]. Depends on the tumor grade and patients' situation, radiotherapy alone or surgical resection follow-by radiotherapy are the mainstays of treatment. Radiotherapy contains external or internal beam radiation. External beam is the most popular treatment and may be delivered as standard external beam or stereotactic. From 1972, attempts to explore radiation therapy beyond conventional doses were initiated. It has been proved that high radiation doses was potentially effective for tumor treatment in different location of the brain since the irradiated patients had significantly longer survival compared with those who treated with lower radiotherapy[6, 7]. However, high radiation dose was also well tolerated and yield normal brain tissue necrosis[8, 9]. Also, in some cases of patients suffering malignant gliomas, especially in grade IV, recurrence may occur within the irradiated volumes or outside the boost radiation therapy[10, 11]. The site detection is significant for treatment assessment for the recurrence could be within or in close proximity to the original site[12]. The reason of the recurrence is variable while the inadequate radiation doses appear to be one of the primary reasons. Therefore, a decision of the suitable radiation dose is critical in the radiotherapy treatments.

Neuro-imaging plays a significant role in clinical analysis and treatments. In the past two decades, people have analyzed quantitatively imaging method for assessing radiation

treatment as well as tumor recurrence after radiation therapy. They include CT (Computed Tomography), MRI (Magnetic Resonance Imaging), PET (Positron Emission Tomography) and SPECT (Single-Photon Emission Computed Tomography). CT is regarded as a moderate- to high-radiation diagnostic technique with high resolution in the image results. Amino acid PET tracers are more sensitive in detecting recurrent tumors, particularly in cases of low-grade tumors[13]. Thus, they are also reliable in differentiating between recurrent tumors and treatment-induced changes. SPECT imaging acquires multiple 2-D images by means of a gamma camera. In our study, we used MRI as a detection tool. It has a relatively wide range of application in medical diagnosis and compared with other imaging methods, it is non-invasive and no contrast agent injection is required. It is quite meaningful in pediatric cases since intravenous access is often problematic.

1.2 MRI

Currently, MRI has been a significant tool for the tumor localization[14, 15], stroke diagnosis[14] and the assessment of the treatment effects. Figure 1.1 has shown one 3 T MRI scanner (Philips 3 T Achieva TX) for human brain examination.

Figure 1.1 3 T MRI scanner(Philips 3 T Achieva TX) for human brain. For different sequences collection, it may takes up to 50 minutes in one time examination. (Picture captured in Kennedy Krieger Institute, Johns Hopkins School of Medicine)

Moreover, MRI has been one of the most common criteria for monitoring response to gliomas treatment, along with the standard Macdonald criteria (corticosteroid dose). The accomplished MR imaging is based on employing water content and water relaxation to image basic anatomy transition inside the organs. The typical application of MRI includes liver lesion investigation[16] and brain tumor analysis. MR imaging of lung is proved to be difficult since the lung consists lots of air, causes a low proton density that leading to a weak MR signals[17]. Also, MR imaging is proved to be helpful during the procedure of stroke treatment[18]. The interaction of the magnetization M with an external magnetic field B in conventional MRI techniques, such as T_1-weighted (T_1w) and T_2-weighted (T_2w) images, can be governed by the Bloch Equation[19]:

$$\frac{\partial \mathrm{M}}{\partial \mathrm{t}} = \gamma(\mathbf{M} \times \mathbf{B})$$

whereγ is the gyromagnetic ratio and $\mathbf{B}(\mathrm{t}) = (\mathrm{B_x}(\mathrm{t}), \mathrm{B_y}(\mathrm{t}), \mathrm{B_0} + \Delta \mathrm{B_z}(\mathrm{t}))$ is the total magnetic field consisting of the main magnetic field B_0, which is constant in time, plus $\Delta \mathrm{B_z}(\mathrm{t})$ which may be time dependent. The latter one is present in magnetic resonance imaging and helps with the spatial decoding of the nuclear MR signal.

1.2.1 Conventional MRI parameters

T_1w depends on the longitudinal relaxation of subjects' net magnetization vector (NMV). Generally, spins aligned in an external field (B_0) are put into the transverse plane by an RF pulse. Then, they return to the original equilibrium of B_0. Since the time cost for different tissues are distinct, T_1 can reflects the amount of time that its protons spins realign with the main magnetic field (B_0). Similar with T_1, tissue with different organization has variable T_2 values while external factor usually has a longer T_2 relaxation time. In MRI, only a single slice of imaged tissue is excited at one time. Slice thickness is typically several millimeters. While to construct a single slice of MR image, it commonly involves collecting a series of frames of data, which is called acquisitions. New transverse magnetization is produced by an RF excitation in each acquisition. Then it is sampled along a specific trajectory in K-space. Basically, a complete MR image can be reconstructed from a single acquisition based on a K-space trajectory which contains a whole region of K-space[20]. K-space sampling pattern is traditionally designed to meet the Nyquist criterion. It depends on the resolution and field of view (FOV). The sample region of K-space also determined the image resolution. A larger region of sampling theoretically leads to

a higher resolution. The FOV also depends on the sampling density within the sampled region. Thus, denser sampling is necessary for larger objects to satisfy the Nyquist criterion. Violation of the Nyquist criterion can result in distortion for the linear reconstruction. The appearance of such artifacts will depend on the details in the sampling pattern.

Currently, both CT and MRI have been the most common criteria for monitoring response to gliomas treatment, along with the standard Macdonald criteria (corticosteroid dose). MRI has been proved to be a powerful non-invasive tool, among which T_1- and T_2-weighted are the widely used MRI sequences. However, there are still some limitations make these conventional MRI methods insufficient: First, gadolinium (Gd)-enhancement based T_1-weighted images may be influenced by radiation necrosis[21] or pseudo-progression[22, 23]. In addition, in case of pseudo-response, the sudden disappearance of Gd-enhancement in the procedure of antiangiogenic therapies cannot detect the recurrence of the tumor[23, 24]. Therefore, tumor barrier determinations simply based on T_1- or T_2-weighted maps are not reliable in every cases[25, 26].

1.2.2 Perfusion and Diffusion MRI sequences

MRI can be divided in two common techniques. One based on arterial spin labeling (ASL) and the other based on dynamic susceptibility contrast (DSC). In addition to the conventional MRI techniques, several advanced functional MRI sequences, including perfusion imaging, diffusion imaging and proton MR spectroscopic imaging have been engage in the clinical research protocols. Recently, a slice of beneficial MRI approaches on the detection of deviation from diffusion behavior have been proposed. For example, apparent diffusion

coefficient (ADC) has been applied in discrimination of tumor, gray and white matter, along with other useful information[27-29]. Also, perfusion imaging of blood flow and vascular permeability can provide crucial clues in measurement of tumor activities[30-33]. Additionally, SPECT and PET are helpful tools to differentiate recurrent tumor and treatment effects[34, 35]. After Macdonald et al. advised a standard for malignant gliomas response assessment[36, 37], it has been worldwide followed and provide a possible availability to evaluate the clinical treatment response. All these imaging techniques provide real-time information about the current state of the brain.

The measurement of Diffusion imaging is based on the variability of "Brownian motion" of water molecules in brain tissue. Brownian motion accounts for the random movement of molecules. Generally, water molecules remain in constant movement state and the rate of movement or diffusion can be explained by the kinetic energy of the molecules and also, it is temperature dependent. Since the tissue has relatively stable structures, diffusion is not actually random in biological tissues. For example, cell membranes, vascular structures, and axon cylinders, are limited or restricted to the amount of diffusion. Also, both chemical interactions of water and macromolecules have an effect on diffusion properties. Therefore, water diffusion is referred to as "apparent diffusion" in the brain. The method to obtain diffusion-weighted images is straightforward. First, a pair of strong gradient pulses is added to the pulse sequence. The first pulse de-phases the spins, and in case the net movement does not occur, the second pulse will re-phase the spins. The signal attenuation will take off once the net movement of spins happens between the gradient pulses. Additionally, the degree of attenuation depends on the magnitude of molecular translation and diffusion weighting. The strength of the diffusion gradients, the

duration of the gradients, and the time between the gradient pulses are the factors to determine and influence the amount of diffusion weighting. The diffusion data can be presented as signal intensity or as an image map of the apparent diffusion coefficient (ADC). Calculation of the ADC requires at least two acquisitions with different diffusion weightings: one is a low ADC corresponds to high signal intensity, the other one is a high ADC leads to low signal intensity on diffusion-weighted images. Slightly hyperintense on diffusion weighted images derives from lesions with prolonged T_2 relaxation times. The detection of this so called "T_2 shine-through" phenomenon can be straightforward from true restricted diffusion on the ADC map since it is the only one to reflect low signal on the ADC map.

Additionally, perfusion character can provide several measurements curve. The time-to-peak (TTP) is the time from the start of the scan until it reaches maximum attenuation. The mean transit time (MTT) is the time cost of the contrast bolus to pass from the arterial side to the venous side of the cerebral circulation. In the condition of a symmetrical attenuation curve, the MTT is given by the first detection of contrast to the maximum attenuation. The integral area below the curve is equal to relative cerebral blood volume (rCBV). Finally, relative cerebral blood flow (rCBF) can be calculated by dividing the rCBV by the MTT. The basic standard for quantitative perfusion imaging is $H_2{}^{15}O$ positron emission tomography. This method is commonly used as a validation for other new techniques[38-40]. The ultimate goal is to decide the absolute cerebral blood flow, but further analysis of arterial input is required. Most methods measure relative blood flow and compare the two hemispheres or the tumor region and contralateral normal brain tissue region for differences.

Although vascular transit time and cerebral blood volume are not as accurately and

clearly to show the interested signals as cerebral blood flow, they are still useful parameters and easily collected on conventional MR systems with a single bolus injection of contrast material. During the dynamic susceptibility contrast (DSC) measurements of MR perfusion, 20 mL of gadolinium is injected at 4 mL/sec. In the speed of 2-3 seconds/slice for 40 second acquisition time, about 13 slices can be collected by an echo-planar sequence in total. Due to T_2* effect, signal attenuation will occur as the paramagnetic gadolinium bolus passes through the cerebral circulation. Moreover, both TTP and MTT are sensitive to hemodynamic changes in the cerebral circulation. Slight increments of these parameters with normal rCBF and rCBV will probably indicate that no brain tissue is at immediate risk of infarction. Generally, the rCBV decreases after rCBF when progresses arterial obstruction. The rCBV initially remains normal or maybe increases because of auto-regulation and dilatation of the capillary bed. If both rCBF and rCBV are reduced, tissue must be assumed. If both of them have significantly reduction, it is probably that irreversible ischemia occurred.

Another MR perfusion method study took off in the early 1990s, which is called Echo-Planar Imaging (EPI) signal targeting with alternating radiofrequency. In this case, each radio-frequency (RF) excitation is followed by a train of gradient echoes with different spatial encoding. Our desirable results of the blood volume map can be obtained by the subtraction of the tagged and untagged images[41].

1.2.3 Amide Proton Transfer

In 1990s, Behar et al. and Kauppinen et al. suggested that several macromolecular

peaks in brain proton MR spectra were discovered in the low-frequency range relative to water. Even if it is known that the aliphatic protons from mobile proteins, polypeptides and lipids make contribution to these signals, the abundant metabolite signals in the proton spectrum caused a complicated explanation for the broad low-concentration resonances. Also, when combined with spectroscopic imaging, the spectra will be with lower spatial resolution than conventional MRI parameters. In addition, if we want to detect these proteins for analysis, the water signal from clinical MRI scanners is necessary. Based on the chemical exchange saturation transfer (CEST) approach, originally investigated by Forsen and Hoffman[42]. It is novel molecular MR imaging parameter that detects the exchangeable protons transition rate between low-concentration chemicals and water[43-45]. In the past several years, some new experimental methods along with its multiple applications on clinical assessments have been proposed, including metabolite detection, pH imaging, imaging of sugars and so on. The CEST encourages the development of new imaging to progress on many fronts.

Zhou et al. used the exchangeable amide protons in the protein backbone in vivo. This technique is called amide proton transfer (APT) imaging[46]. Amide protons (-NH) in the backbone of solute proteins have high resonation (around 8.25 ppm) in the proton MR spectrum, which is about 3.5 ppm downfield of the water signal. The difference can lead to chemical exchange of water proton by interaction. Previous study has shown that the pH condition decide the exchange rate of the protons which typically reduces pH drop[47]. Based on the mechanism of these endogenous cytosolic proteins and peptides in biological tissue made with a group of CEST agents, a novel protein-based APT imaging technique has been developed. A pulse sequence which is similar to standard magnetization transfer experiments is able to acquire APT

signals[48]. In addition, the APT effect can also be detected as a reduction in bulk water intensity thanks to the proton exchange of water with labeled backbone amide protons of endogenous mobile proteins. Figure 1.2 shows the principle of the APT signal enhancement.

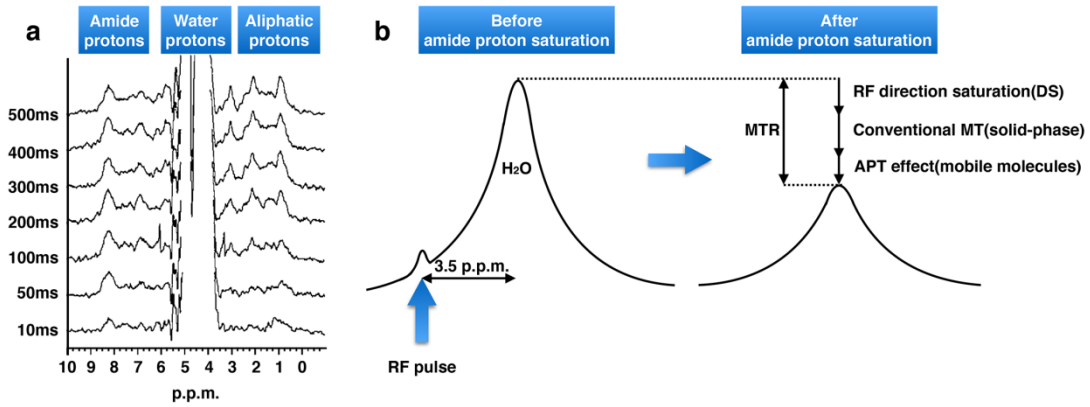

Figure 1.2 APT signals enhancement principle. (a) Water exchange (WEX) spectra for *in vivo* rat brain as a function of mixing time after water magnetization labeling. (b) APT signal changes instruction. The exchangeable protons transfer happens between dilute amide protons and water protons. The RF irradiation saturated amide protons would exchange with unsaturated water protons in next step. Then these protons become saturated and the process will repeat. The bulk water signal will decreases significantly as the saturation transfer if the saturation time is long enough and leading the detection of low concentrations.

As mentioned above, APT is determined by exchange between water feasible amide protons and mobile proteins and peptides. Under the condition of saturated endogenous mobile proteins, APT has a negative change in signal intensity of the free water[49, 50], leads to a contrast-enhancement. In contrast with conventional MRI methods, namely T_1w and T_2w, APT along with diffusion-weighted images, typically ADC and perfusion-weighted blood flow, can be more sensitive in evaluating the gliomas response to therapy and potentially allow a more accurate and predictable clinical assessment[51, 52]. Uses of automatic or semi-automatic methods

on ROI determination have been implemented and developed. These algorithms significantly increase the accuracy of the localization of brain tumors or reach more stable extraction results[53-57], plus they are more time-saving methods than manual ones.

The present study attempted to offer a semi-automatic method for the ROI extraction on APTw images to compare with the manual segmentation by experts, under the similar experiment platform with previous study[52], making an effort to derive more explicit details for the assessment of gliomas therapy response by quantitatively comparing different MRI parameters.

1.3 Image Segmentation Algorithms

Image segmentation has been applied in medical image acquisition methods including MRI, CT, PET, SPECT, and so on. Brain image segmentation of MRI is able to specify the type of tissue for each pixel or voxel in a 2D or 3D dataset. Combine this information with the available knowledge of brain, the medical researches and investigation can go on wheels. As the "Big Data" time has come, the increasing amount of medical images need more effective use of computer application in facilitating their processing. To assist clinicians in their treatments of patients, literatures on MRI applications of image segmentation has flourished. Unsupervised image segmentation algorithms have matured to the point where they generate reasonable segmentations, and thus can begin to be incorporated into larger systems or study support. The time has arrived for these segmentations to play a more important role in brain tissue recognition, for example, white and gray matter separation of the brain, tumor extraction from the normal

brain tissue, as well as the other structure investigation of the brain[58]. The condition changes in the composition of these brain tissue (for both substance or particular location) happened and detected by these MRI, can be used to investigate physiological processes and disease severity[59] or disease entities[60]. It can also be applied in quantification of tissue volume, visualization and analysis of anatomical structures, surgical planning, and surgical navigation. Generally, the brain image has a complicated structure and it always contains artifacts including noise, partial volume effect and intensity in-homogeneity which is not actually should be shown in the real condition.

It has been widely accepted that the existing segmentation algorithm can be categorized into region-based segmentation, data clustering, and edge-base segmentation. In our study, we implemented both region-based level-set method and segmentation with thresholding method. The traditional region-based image segmentation algorithms depends on the homogeneity of the image intensities in the ROI[61]. In cases of intensity in-homogeneity, it cannot give accurate results[62]. Level-set methods take the energy minimization into consideration. Thresholding method is one of the conventional methods in the segmentation method. It has some advantageous characters including relative stable performance, straightforward calculation with high efficiency that make thresholding method remain to be one of the most popular algorithms in this field. The thresholding methods take the histogram of gray level for the pixels into consideration, which is determined by the theory of iteration. Sometimes, we need one or more thresholds for our different segmentation objectives, which have been defined as bilevel[63] thresholding and multi-thresholding[64]. However, all thresholding methods have a common limitation: in case that the histograms cannot show clear valleys, then the threshold is hard to

decide. In order to avoid the drawback of hard thresholding method, we limited the objective region in advance. Human interaction of initial condition in advance can be more believable than purely automatic examination. Additionally, we compare the results from automatic method in the whole procedure with those results of semi-automatic method and manual ones.

1.4 Background and thesis objective

Aim 1: Compare multi-parametric MRI values in the examination of U87 tumors. In our study, we have calculated T_1, T_2, ADC, blood flow, MTR and APTw signals for the tumor region. Also, the contralateral normal side of brain tissue was investigated. By analyzing the difference and ratio between tumor side values and contralateral normal brain tissue, we can detect how the conventional, perfusion and diffusion MRI as well as APTw signal intensities behave at different time points of preradiation and postradiation. This allows us to estimate how much details can be reflected from the different MRI parameters, and make comparison for these parameters in postradiation assessment. Therefore, even though surgical pathology analysis is not advised during the whole procedure of the radiotherapy assessment, by analyzing different parameters, we can detect how much information can be collected for post-radiation therapy so that improve the accuracy of differentiating the treatment necrosis and tumor recurrence.

Aim 2: Implement the automatic and semi-automatic segmentation methods for ROI extraction. Currently, manual segmentation is commonly used in similar procedure. In our study, we collected the data at different time point, used both the automatic and semi-automatic methods and compared them with conventional manual method for both efficiency and accuracy.

We chose level-set algorithm as an automatic method and thresholding method with user interaction as the semi-automatic one. The tumor extraction results from all methods will be shown in the following chapter and discussion afterward. The inter-rater and intra-rater for manual and semi-automatic methods analysis will be implemented in the discussion. Thus, applying semi-automatic methods in the ROI extraction step of image analysis, it is potentially more time-saving with a stable and accurate conclusion from different raters.

2. Materials and Methods

2.1 Rat tumor preparation

All experimental procedures were under the permission of Johns Hopkins Animal Care and Use committee. In 13 T-cell deficient nude rats (20-22 weeks, 300-350 g), highly malignant anaplastic U87 gliomas were clone inside. During the tumor cell implantation, all of them were induced anesthesia through intraperitoneal injection of solution (3-5 mL/kg) which contains ketamine hydrochloride 25 mg/mL and xylazine 2.5 mg/mL. In order to set accurate and consistent positions, we first set a mark on the scalp incision showing the sagittal and coronal sutures. Then, a needle was inserted into the burr hole, which was set by an electric drill, approximately positioned at 1 mm anterior to the coronal suture and 3mm right to the sagittal suture. Next, at the depth of 5 mm from the skull, we injected each rat of U87 gliomas cells (1 million in 4 μL media) for over 3-4 min. Finally, we used the wound clips to suture rat skull. All rats underwent one MRI examination before the initial radiotherapy and then, 6 of them were observed 1, 4, 8 days after radiation therapy, 4 of them were observed at 4 days, 2 of them were scanned at 4, 8 days post-radiotherapy. One of the rats died before second examination at 4 days post-radiotherapy.

2.2 Radiotherapy

After 11-13 days of the tumor implantation, the tumors had grown the size of 4-6 mm in

diameter and all 13 rats were taken therapy by micro-bubble first and then irradiated by a small-animal radiation research platform. The rat head and body was fixed with a specific device in the whole procedure to avoid motion artifacts. First, all rats were anesthetized by 4% isoflurane which last 5 min and kept to be in the 2%-2.5% isoflurane environment in the following radiotherapy. Next, micro-bubble was delivered after dispensed through a direct injection of tail vein. Finally, with the guidance of on-board, cone-beam CT image, dose of 8 Gy well-collimated X-ray beams with 10×10 mm^2 area was administered to the center of the tumor.

2.3 MRI protocol

All imaging were performed on a horizontal bore 4.7 T MR Imaging System (Bruker Biospin), collected at several time points. The equipment picture has been shown in Figure 2.1.

Figure 2.1 4.7 T Magnetic Resonance Imaging System (Bruker Biospin). Enough space for rat or mouse's examinations.

Six MRI sequences have been used with the following parameters: T_1 (inversion recovery, pre-delay = 3 s, echo time (TE) = 30 ms, inversion recovery times = 0.05, 0.3,0.6,1.2, 1.8, 2.5 and 3.5 s, number of averages (NA) = 4), T_2 (repetition time (TR) = 3 s, TE = 30, 40, 50, 60, 70, 80 and 90 ms, NA = 4), isotropic ADC (TR = 3 s, Te = 80 ms, b-values = 0, 166.7, 333.3, 500, 666.7, 833.3 and 1000 s/mm^2; NA = 8), blood flow (Arterial Spin Labeling [ASL], 3s labeling at a distance of 20 mm away from the imaging slice, TR = 6 s, TE = 28.6 ms), APT (Radio Frequency (RF) saturation frequency offsets of ± 3.5 ppm, TR = 10 s, TE = 30 ms, saturation power = 1.3 μT, saturation time = 4 s, NA = 16) and MTR (RF saturation frequency offsets of 10 ppm, 2000 Hz at 4.7 T, TR = 10 s, TE = 30 ms, saturation power = 1.3 μT, saturation time = 4 s, NA = 16). They were all using single-shot, spin-echo, echo-planar imaging for image acquisition

(field of view (FOV) = 32 × 32 mm^2, matrix = 64 × 64). Finally, high-resolution T_2w images on both axial and coronal were given by the parameters of TR = 3 s, TE = 64 ms, thickness = 1.5 mm, NA = 2, and FOV = 32 × 32 mm^2 , matrix = 192 × 192 on coronal plane, and FOV = 42 × 32 mm^2, matrix = 256 × 192 on axial plane, with overall 5 slices in total for each rat at each time. During the MRI scan, all rats were anesthetized with 5% isoflurane in a mixture of 75% air and 25% oxygen for sedation, followed by breathing 1.5%-2.0% isoflurane through a nose cone. Rats in the magnet were monitored online through a small-animal respiratory-gating system connected with a fiber optic cable, and the breathing rate of the animal was kept at 40 ± 5 breaths per minute by adjusting the isoflurane ratio.

3. Image Analysis

The authors have chosen MATLAB (The MathWorks, Inc., Natick, MA) in house script as the working environment for its friendly human–computer interaction design. For a clear comparison result, T_1, T_2 and ADC maps were calculated as followed: $I = A + Bexp (-TI / T_1)$, $I = I_0exp (-TE / T_2)$, and $I = I_0exp (-b \times ADC)$. The original APT signal was fitted by the difference of MTR values at ± 3.5 ppm relative to the water signal, which defined as $MTR_{asym}(3.5\ ppm) = (S_{sat}(-3.5\ ppm) - S_{sat}(3.5\ ppm)) / S_0$, where S_{sat} and S_0 are the signal intensities with and without radiofrequency irradiation.

The ROIs on tumor and contralateral side of brain tissue were drawn by two experienced reviewers (namely Rater A and Rater B) in neuro-oncology imaging, independently performing the manual and semi-automatic methods on APTw maps. Rater A and rater B were respectively with one- and four- year experience of ROI drawing. The normal contralateral side of the brain tissue was used as a comparison. Then the mask of consistent sites was transferred to other co-registered MR imaging results. The lesions of the tumor which had shown abnormal MRI signals were mostly covered in the ROI areas while the ventricles and peritumoral edema were not considered.

3.1 Image segmentation applied on ROI

Brain tumor segmentation from MRI biomarkers has been proved to be a difficult task since it involves variable size, irregular shapes, unpredictable locations, or showing different image intensity or gray levels. Because of some reasons such as necrosis, edema, the tumor

structures may deform which can change the signal intensity properties of the inside or outside regions of the tumors. The traditional manual segmentation is a difficult and time consuming tasks even for the experienced experts which makes an automatic or semi-automatic brain tumor extraction method desirable[65]. Automatic methods of brain tumor extraction can provide many possible application, such as surgical planning, treatment planning and vascular analysis[65]. Particular characteristics in pathological regions of brain can be reflected in blood vessels[66, 67].Along with vascular analysis, the objective and reproducible MRI segmentation can allow us to have a deep insight about the relation between pathologies and blood vessels and may develop a new diagnostic measure. Among all the segmentation algorithms, even though variety of them have been discussed, their purpose are quite the same as Gestalt principles of perception, including simplicity (minimum description length), similarity (homogeneity of semantic regions), as well as continuity, proximity and closure. By means of various mathematical tools, the images are partitioned according to different rules for variety of algorithms.

3.2 Different methods implement

3.2.1 Manual segmentation:

The experts were asked to outline the margin of the tumor on each APT slice, with the help of information from other MRI signals (especially ADC) when necessary. The area in the contour was defined as the cross-section areas of the tumor obtain by APT maps. Since the whole contrast-enhancing tumor were defined as tumor area, so it contained all tissues including

non-enhancing tumor and necrosis (inside or outside the contrast-enhancing tumor). Consuming time of manual segmentation was recorded by one of the experts.

3.2.2 Automatic level-set method

Original level-set methods were introduced by Osher and Sethian which are numerical techniques to trace moving interfaces[68]. After the mathematic theory was applied to image segmentation problems, it supports the technician to derive implicit and non-parametric representation of the image contour. According to the level-set theory, the contour is the intersection of the level-set function with the 2D image of x-y plane, and set the zero level on a new dimension which is defined based on the image plane. To keep the numerical robustness, the level-set formulation can maintain automatic change in the topology of contour. In principle, segmentation is obtained by minimizing an objective function (proposed in advance) either by discrete or continuous formulation of calculus of variations. Regarding the level-set methods, Bayesian statistical inference formulation can bridge the discrete and continuous approaches. Suppose we have an image I(x) and we would like to infer the delineating curve C between an aiming object and its background. It can be achieved through maximizing the probability distribution function (PDF) P(C|I), using Bayes law[69]:

$$P(C|I) \propto P(I|C)P(C)$$

The prior probability P(C) will be reformulated to have "syntactic" and "semantic" components. Classical active contours methods, such as the snake algorithm of Kass et al.[70], use parametric

representation C = C(p). In this formulation, it has been divided into two terms:

the "external force" term

$$-logP(I|C) = -\lambda \int |\nabla I(C(p))| dp$$

and the "internal force" term

$$-logP(C) = \int (\alpha |Cp|^2 + \beta |Cpp|^2) dp$$

The maximization over all possible separating curves[71] is done by minimizing the result of

$$-logP(C|I)$$

In addition, the prior part dictates the degree of smoothness of the curve so it is not directly related to the cluster classification of images or objects. The segmenting curve C is represented implicitly using the level-set framework[68]. There are many applications of extracting complex object boundaries from unrelated background have been successfully implemented for this curve evolution, result in an advanced development in the topology. Moreover, the image level-set function indicated continuous, multi-shape representation enables a definition of a unique dissimilarity measure between object views.

3.2.3 Semi-automatic method

Among all the suggested techniques in image segmentation, thresholding is the convenient approach which can separate the objects from the background in concept. Thresholding convert an image into a binary image based on a threshold value "t". Once the gray level of the pixels is below "t", it would be marked as black (background), which others would

be represented as white (aiming object). In the ideal condition when the objects and background have dissimilar intensity distributions, thresholding methods will work pretty well. Therefore, in the whole procedure of thresholding methods, the principle is to find an ideal threshold value (in cases of multi-thresholding, there will be several thresholds). In this procedure, thresholds can be set either manually or automatically. For instance, in case of manual settlement, by human interaction, one specific pixel can be chose and set its gray level as a threshold. In case of automatic settlement, we can decide a threshold by statistic or other mathematic theories. For the former ones, errors may happen in selection of "t" and later more problems are produced in image analysis. In our thresholding method, the peaks and valleys were searched in the histograms and set the thresholds based on them. If the histogram is noisy and false minimum and maximum are detectable, the segmentation mistakes will occur. To let algorithm based on peaks detection be smoothed and significant peaks is clear enough to be found, one algorithm based on peaks detection suggested by Sezan[72], 1985 which at first finds zero-crossings and later uses a peak detection signal to estimate significant peaks. One advantage of this method is that it can adjust the performance of the peaks by human interaction. Moreover, one famous thresholding algorithm is Otsu's method suggested in 1979[73]. In this automatic unsupervised thresholding algorithm, distribution of pixels value is analyzed. The basic idea of this method is that the similar pixels should be classified into same cluster. This means that the variance inside each class should be minimized or it can be explained as energy minimization. Otsu defined the within-class variance as the weighted sum of the variances of each cluster. Minimizing within-class variance has same effect with maximizing between-class variance. Therefore, after being applied in many cases, Otsu's method is widely employed in literature and its result is

robust and satisfactory. Further discussions for thresholding are based on information theoretic approach which was introduced by Pun in 1980[74]. The entropy-based techniques have proven to be successful and convincingly robust[75-77]. These techniques rely on maximizing the total entropy of both the object and background regions to discover the suitable threshold.

Gray level thresholding is simple to grasp and fast to construct, however, the threshold selection itself is not always straightforward. The major drawback of threshold-based approaches is that they often fail to find the best separation between the object signals (true ones) and background signals (false ones or noise). In case that the threshold is kept too low, a lot of desirable signals may not be detected. Therefore, we combine the manual segmentation in the first step in order to give an initial condition for a more accurate thresholding calculation.

The semi-automatic methods were used to be implemented in T_1w images[53, 78] while it is a novel idea on ROI extraction of tumor based on APTw maps. The method began with the roughly manual extraction on tumor region. The experts outline an enlarged contour outside the contrast-enhanced areas without indispensably pointing out the details of the tumor edges. Then the original tumor mask was produced and automatically processed in the second-stage. Based on the intensity difference between contrast-enhanced areas and normal brain tissue, previously described entropy thresholding techniques[79] were used to identify our targeting ROI. In addition, the morphology process was implemented for image de-noising. The overall flowchart of the semi-automatic method is shown in the Figure 3.1.

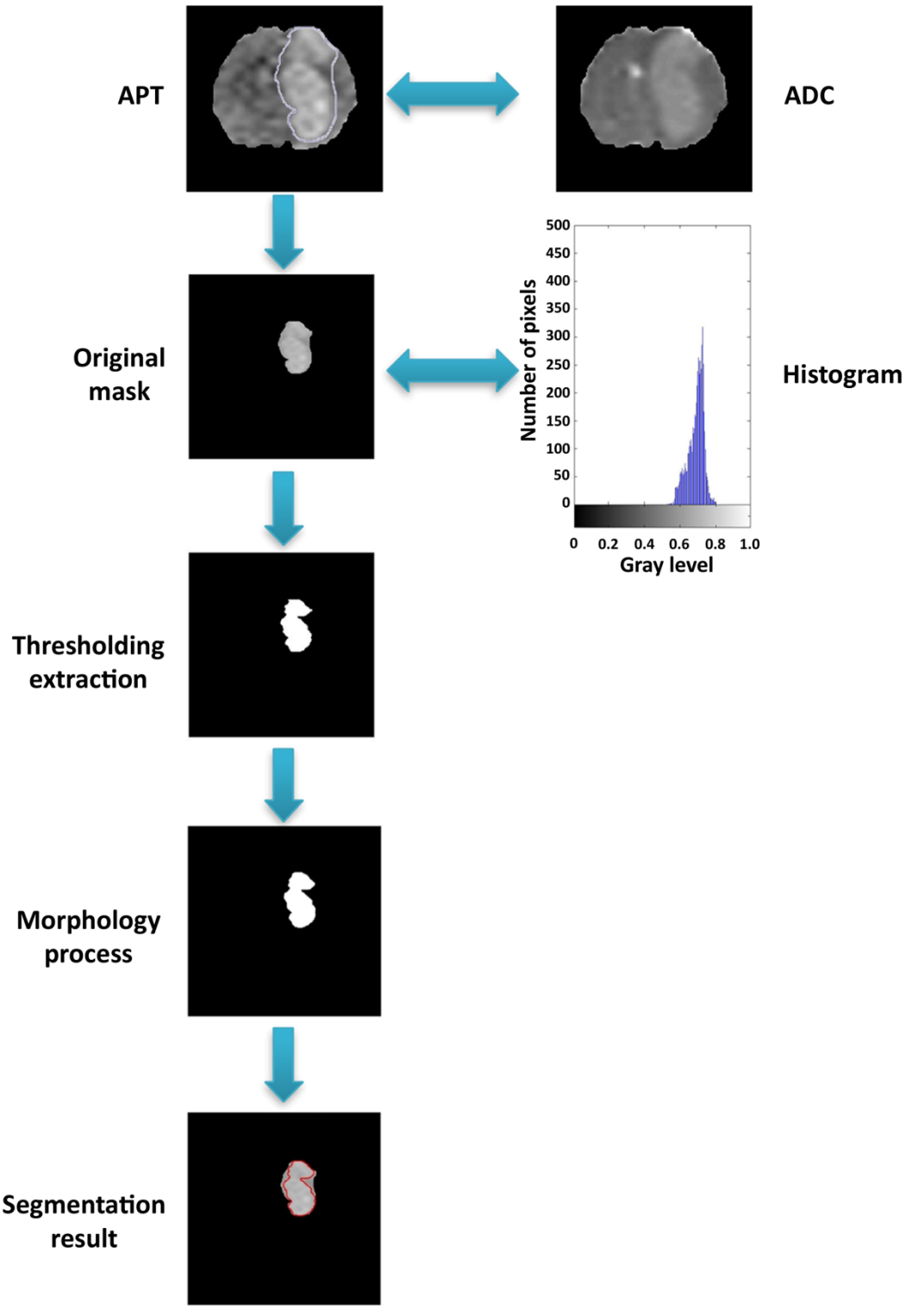

Figure 3.1 Flowchart of semi-automatic tumor region extraction method for one sample. First, human interaction of initial ROI extraction on APTw map. If necessary, co-register the information from ADC map. Second, take histogram into consideration and label the original mask. Next, de-noise the temporary result by morphology process. Finally, highlight the contour.

Figure 3.2 shows the ROI extraction results derived from original image (a) by three different methods, namely manual method (b), automatic method (c) with level-set algorithm (multi-phase) and semi-automatic (d). The manual method and semi-automatic method gave more accurate results than automatic method. The level-set method is based on differences of the independent regions. Since the blurring edge of the tumor can transit smoothly, the algorithm will have a high chance to separate the blurring areas into common cluster. Therefore, even if automatic level-set method can sometimes detect the edge of the ROI clearly, it may fail in the cases with blurring edge.

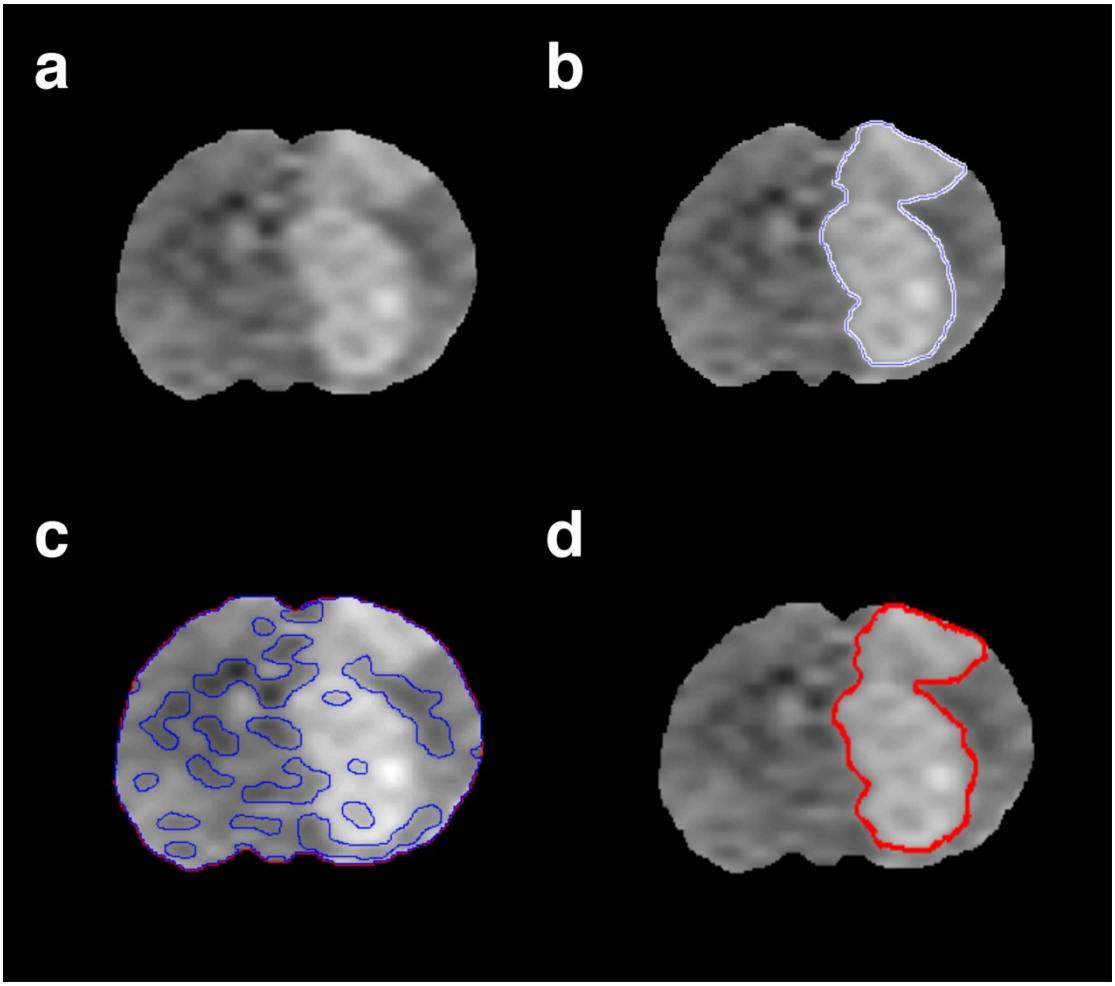

Figure 3.2 Region of interest extraction results from three methods. Given the original APTw map (a),manual (b) and semi-automatic methods (d) can achieve accurate ROI extraction results. Level-set algorithm based automatic method (c) can hardly accurately confirm the contour of the tumor region.

4. Experiment Results

4.1 Statistical Analysis

The results from all MR Imaging were described as mean ± SD. The tumor areas obtained from APTw maps were assessed with the intra-rater and inter-rater reliability described by Bland-Altman[80] and the mean with ± 2xSD has been labeled in the figures. Based on the calculation of difference against mean, the agreement between the two sets of mechanism was then examined. The p values below 0.05 obtained by two tail t-test were considered significant. Measurement artifacts may exist in the human observers in clinical assessments, for example, a clinical assessment conducted by a physiotherapist, or the instrument used such as a goniometer[81]. In our study, we focus on the issue of determining the reliability of the human observer or in the case of semi-automatic method with computer-aid algorithm, which is the ability of different observation methods to produce the same measurements under the same conditions with the consistent sample[82, 83] . Two terms of observer reliability are discussed:

•intra-observer (or within observer) reliability - the degree to which measurements taken by the same observer are consistent

•inter-observer (or between observers) reliability - the degree to which measurements taken by different observers are similar.

Accurate assessment of tumor response to treatment for patients plays an important role in determining whether the clinicians should continue the current therapy or choose an alternative therapy. Intra- and inter-rater reliability analysis is helpful in comparing two different

methods for one common subject. The verification of the exact location of the tumor is fairly difficult to determine. It requires the pathology examination for different time point. During the monitoring of the tumor growth procedure, tissue sampling via surgery is not allowable for every part of brain for *in vivo* subjects. Even if then surgery is possible and being advised for the patients, choosing the area to target for tissue sampling is quite hard since the gliomas are heterogeneous. Therefore, more agreeable and reliable imaging parameters that can distinguish between real tumor progressions and treatment effects such as necrosis caused by treatments are urgently needed. By analyzing the intra- and inter-rater reliability, how the methods works different from each other, in the aspects of efficiency, stability for single or different experimenters, and which method can achieve a more consistent result, all can be concluded from the comparison.

4.2 Morphological Features of Irradiated Tumors

The planned observations were operated with MRI after 11-13 days post-implantation. These tumors had grown as 3-7 mm in diameter pre-radiotherapy. The T_2w MRI characterized that after 8 Gy radiation therapies of all rat tumors, they were still growing in size during the following examinations. Three of the tumor growths have been shown in Figure 4.1(a). The transition of the tumor cross-sectional areas obtained from the APTw maps is shown in Figure 4.1(b) for all the rats. At different time stages (on 4 days and 8 days post-radiotherapy), the areas showed significant difference ($p < 0.01$).

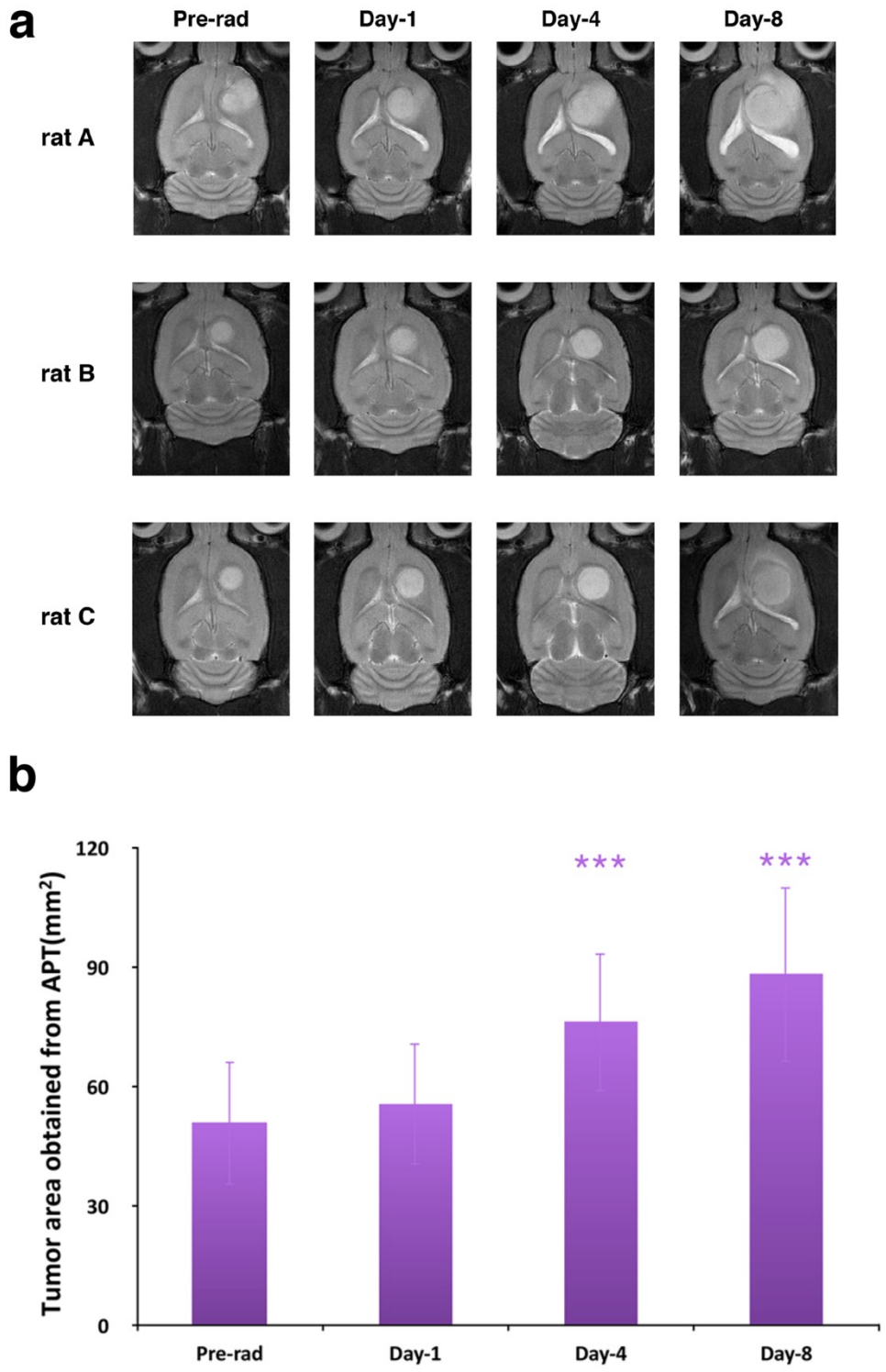

Figure 4.1 The representive anatomy image of rat A, rat B and rat C, and the tumor area comparison for the entire group. (a) T_2w MRI features investigated at different time points of pre-radiotherapy, 1 day, 4 days and 8 days post-radiotherapy for 3 different rats. The irradiated tumors were still growing in size during the postradiation development. (b) Tumor cross-section areas obtained from the APTw maps at different time point of preradiation, 1 day, 4 days and 8 days postradiation. The statistical significance of the difference compared with preradiation: *p < .05, **p < .01, ***p < .001.

In the procedure of semi-automatic method implement for brain tumor extraction, morphological process was induced in as a second step of the tumor extraction. In the first step of automatic part, thresholding segmentation helped to separate the object from the background. However, because of the unstable properties of tumor and variety of brain tissue condition, noise will exist after first stage segmentation. Thus, in order to de-noise the signal of the APTw maps, we used the morphology process in the following two steps of after thresholding. For the first step, some spots noise outside the main part of the tumor region was deleted. Even if there might be some detail lost on the edges of the region of interest, it successfully save important information and kept a low noise percentage after the procedure. In the second step, necrosis existence after radiotherapy was taken into consideration. The necrosis part of the tumor shows contrast signal from the effective tumor region. In the APTw images, it will show hypointense signals in the necrosis part of the tumor.

4.3 Multiparametric MRI of Irradiated Tumors

Figure 4.2 shows that in the maps of T_1, T_2, ADC and APTw, the tumor was hyperintense compared with the normal tissue on the contralateral side of the brain, while it is hypointense in MTR maps. Imperceptible changes throughout the time points on T_1 and T_2 maps can be detected. In contrast, on the maps from ADC, blood flow and APTw, we can detect significant difference between pre-radiotherapy and post-radiotherapy. On the blood flow maps, both the tumor and contralateral part of the normal brain tissue had clear signal intensities. As studied before, the tumor remained to be hypointense from preradiation to postradiation[52]. The

signal intensity of lateral 3 time points (1 day, 4 days and 8 days) after radiotherapy decreased significantly compared with the time of preradiation. However, on the ADC maps, the intensity of tumor region of the brain increased in postradiation time points and become very hypointense at 8 days post-therapy, leading to a clear contrast with contralateral part of the normal brain tissue. On the APTw maps, the signal intensity had a decrease in post-radiation observations, similar to blood flow. At 8 days after radiation therapy, it gained a maximum difference compared with preradiation, resulting in a close intensity with other normal part of the brain.

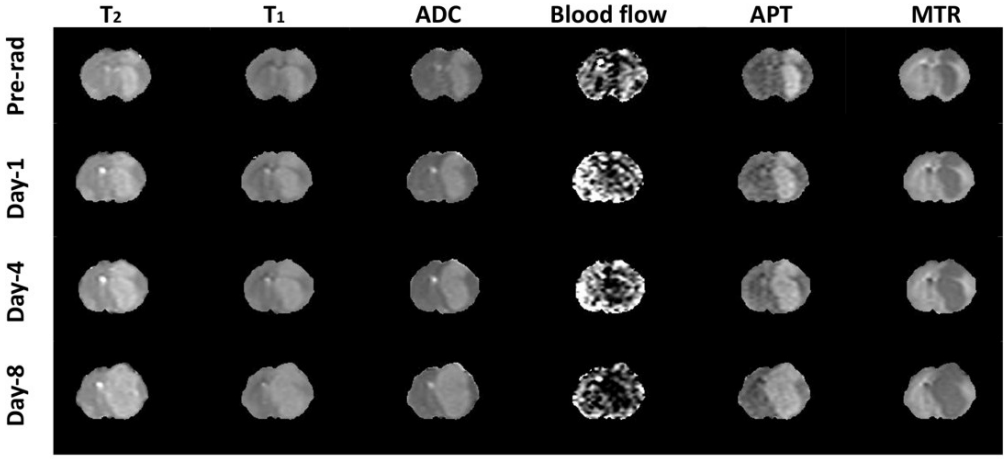

Figure 4.2 Biomarkers of T_2 (0 - 100 ms), T_1 (0.5 - 2 s), ADC, blood flow (0 - 200 mL/100 g/min), APTw (-10% to 10% of the bulk water signal intensity) and MRT at 2 kHz (0% - 50% of the bulk water signal intensity) changes at different time points of preradiation, 1 day, 4 days and 8 days postradiation for one single rat with a U87 MG glioma. The outside noise of brain tissue has been filtered.

Figure 4.3 presents the longitudinal comparison among quantitative analysis of the MRI signals of the irradiated tumor. In T_1, T_2 and MTR maps, there was no substantial changes throughout the observations both during pre-radiation and post-radiation. Furthermore, it indicated that the average ADC values had a steady increase during the examinations. It showed a clear increment from preradiation ($1.05 \pm 0.01 \times 10^{-9}$ m^2/sec) to the first day postradiation ($1.09 \pm 0.02 \times 10^{-9}$ m^2/sec). Although it had a slight change to $1.10 \pm 0.03 \times 10^{-9}$ m^2/sec at the 4 days,

there was again a great increase in 8 days ($1.15 \pm 0.05 \times 10^{-9}$ m^2/sec). The observed blood flow signals in tumors were lower than those in contralateral parts of the brain tissue during the time of post-radiotherapy. In the post-radiation imaging, the average blood flow values in the tumors decreased with a high difference compared with the pre-radiation even though there was a peak at first day after radiotherapy (78.9 ± 22.6 for 1 day, 49.8 ± 24.3 for 4 days, 38.6 ± 22.5 mL/100g/min for 8 days, compared with pre-radiation for 64.8 ± 20.5 mL/100g/min, leading to p = 0.0400, 0.0066, 0.1060 respectively). Similarly, even if there was a growth in the 1 day examination, the values of APTw also reduced in the whole procedure of post-radiotherapy (2.82% ± 0.30 vs. 3.01% ± 0.50% with p = 0.4568 as 1 day, 2.37% ± 0.37% with p = 0.0111 as 4 days and 2.10% ± 0.26% with p = 0.0037 as 8 days). In contrast, the APTw showed an opposite change tendency compared with the tumors in the contralateral side of the brain tissue.

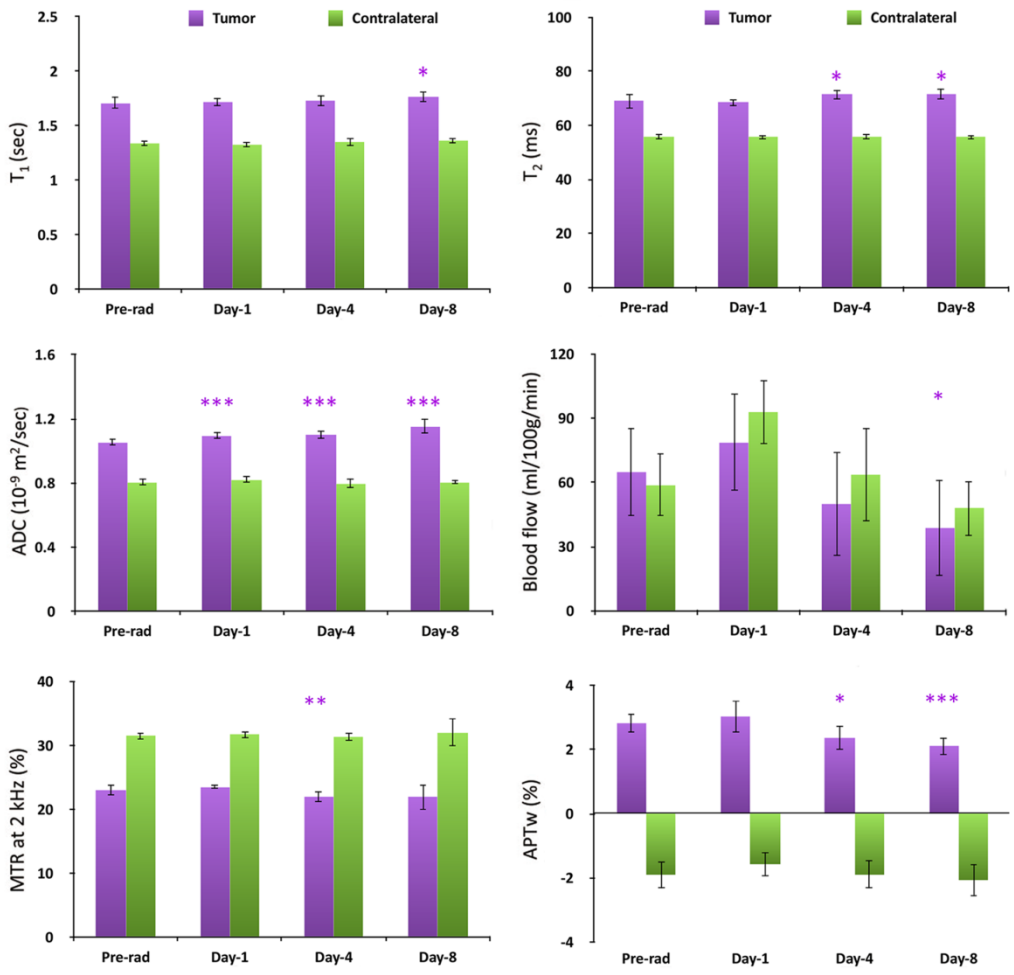

Figure 4.3 Multiparametric MRI biomarkers of tumor analysis at different time points of preradiation, 1 day, 4 days and 8 days postradiation. The statistical significance of the difference in relative to preradiation: *p < .05, **p < .01, ***p < .001.

The relative changes of MRI values analyzed in quantitative were also shown in the Figure 4.4. The plots of blood flow and MTR signal intensities changes in tumors with respect to contralateral side of the normal brain tissue were given by their ratio while others were obtained by their differences. In most of the conditions, the statistical significances are corresponding to those in relative MRI intensity differences, which all of them were gained by post-radiation compared with pre-radiation. In contrast, relative blood flow changes had an opposite change tendency. The 8 days post-radiation had a significant difference on original values while 1 day

and 4 days post-radiation had high p values for relative differences.

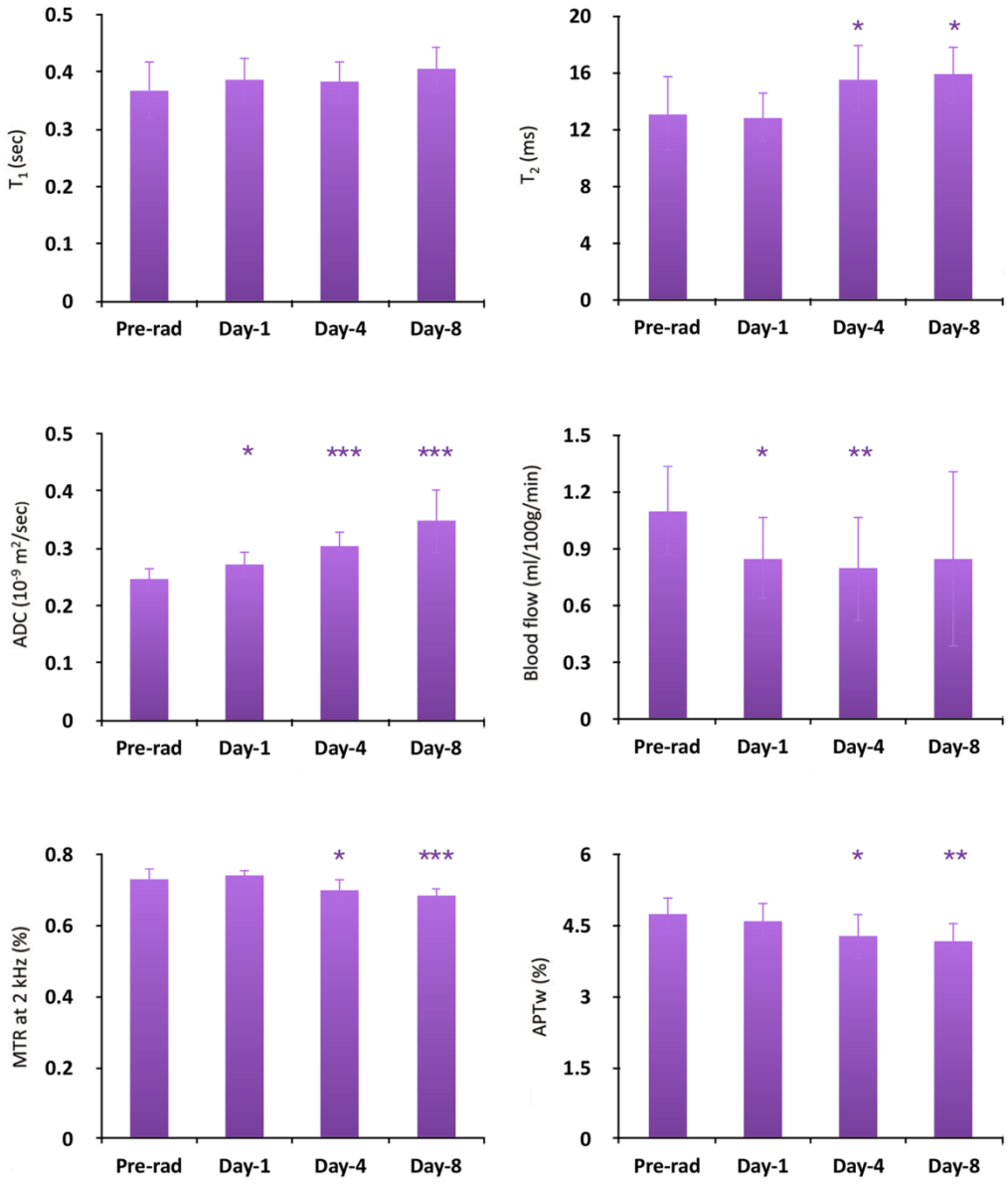

Figure 4.4 Multiparametric MRI signal intensities of tumor with respect to contralateral normal brain tissue analysis at different time points of preradiation, 1day, 4days and 8days postradiation. The statistical significance of the difference in relative to preradiation: *p < .05, **p < .01, ***p < .001.

4.4 Histogram Analysis

The histograms distribution in Figure 4.5 shows the multi-parametric MRI values change of one specific irradiated rat, demonstrating the status and size variation of the tumors. After irradiation, the tumor size continued to grow, and the histograms shifted. For instance, the ADC indicated a right shift after radiation therapy, just as discussed before[52]. In contrast, the peaks of blood flow and APTw histograms had a steady left shift during the procedure of the tumor development. The other three histograms, T_1, T_2 and MTR, however, didn't show a distinct change from the pre-radiation to the post-radiation.

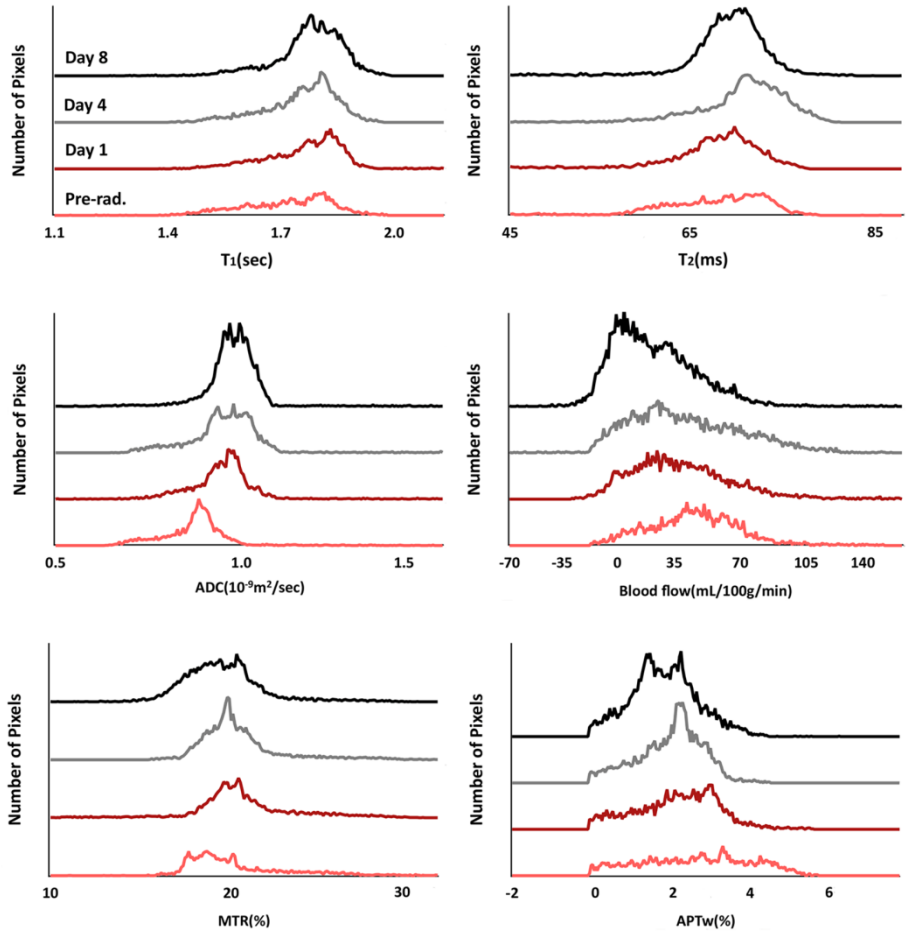

Figure 4.5 Histogram analysis of multiparameteric MRI biomarkers at different time points of preradation, 1 day, 4 days and 8 days postradiation for U87 MG glioma in a rat. It shows that ADC histogram had a right shift while blood flow signals and APTw intensity had a left shift after radiotherapy.

4.5 Semi-automatic method evaluation

To assess the results of the semi-automatic and manual methods, we evaluate the inter-rater and intra-rater reliability of ROI extraction. At the beginning, all tumor masks required an initial and broader condition. The most frequent errors were due to suboptimal brain extraction caused by, for example, the blurring parts, especially those transition areas close to the ROI. For the edges with high contrast ratio, even if there was much details and irregularity, the contour could be drawn broaden. The mean time for initial condition decision was 45 s (range from 5 s to 1 min) per scan. The followed automated step of the generation to a tumor mask consumed 20 s of computer processing time with a standard personal computer (2.90 GHz CPU, 8 GB RAM). Therefore, the overall average time required for production of one single tumor mask was about 1 min. The reviewer that recorded the used time for manual method was 5 min per examination, which also considering the incorrectly drawing and reproduce consuming time (since the manual method required more detail detections, causing high chance of retesting thanks to mistakes).

4.5.1 Intra-rater reliability trial

The second time measurements of both manual and semi-automatic methods were conducted one week after the first time. There was a slight difference in the Test 1 (manual method) measurements for rater A ($p_1 = 0.0161$) while Test 2 (semi-automatic method) measurements ($p_2 = 0.7081$) had no significant difference. The test results were displayed in Figure 4.6 (a and b).

For the personal bias, sight and hand vibration errors at different periods, the agreement between the two ratings was fair-good by visual estimation on the figures. The collected data mainly distributed close to the midline of the y-axis (difference against the mean). This reflected that the same person tends to give the similar results at different time, leading to a more stable ROI extraction results.

4.5.2 Inter-rater reliability trial

Before the semi-automatic method was conducted, both of the raters were trained by 10min session on familiarizing with the test procedure. This session was about introducing the interaction procedure with the program and emphasizing the raters on pointing out the blurring areas of the ROI. Then Rater A and Rater B independently implement both manual and semi-automatic measurements of ROI. The manual method had a more scattered distribution as displayed in Figure 4.6 (c and d) by estimation. Also, the p values showed that manual method ($p = 0.0000$) had significant difference between two raters while the results of semi-automatic method kept to be stable ($p = 0.1464$).

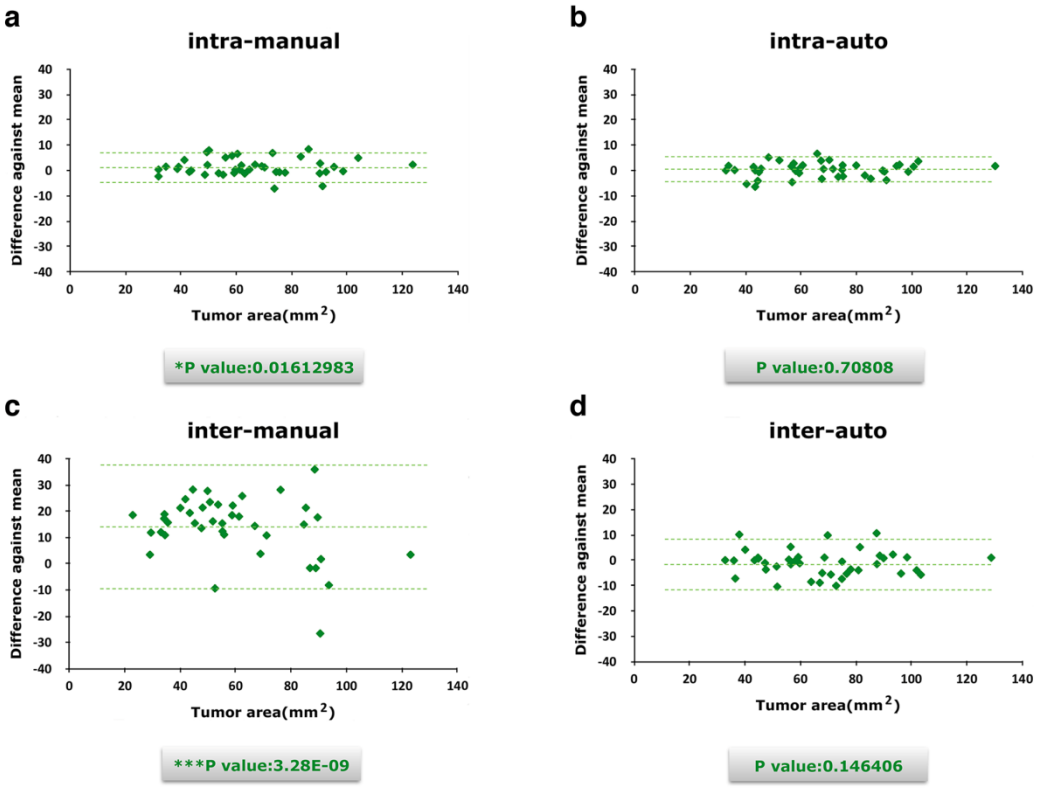

Figure 4.6 Intra-rater (a and b) and inter-rater (c and d) analysis comparison between manual and semi-automatic ROI extraction. It demonstrated that manual segmentation had a wider contribution than semi-automatic method in both inter- and intra-rater experiments.

For the personal bias, sight and hand vibration errors from different raters, the agreement between the semi-automatic ratings works was fair-good. The data kept to distribute close to the midline of the y-axis showing that this method remained stable in the condition of drawing ROI from different people. In the situation of inter-rater, manual method was more likely to have personal bias and errors, leading to unstable results of the ROI. Even if raters had same detection and judgment of the ROI boundary, they might still have different conclusion of the areas because of manual drawing errors.

5. Discussion and Conclusion

5.1 Discussion

The pathology analysis on tumor is the only reliable method to assess the tumor response to ongoing treatments. However, tissue sampling via biopsy is not feasible for all brain areas. As well as the gliomas are heterogeneous, it is still difficult for distinguishing between the tumor region and tumor progression. To find more reliable imaging parameters for clinical need, including perfusion and diffusion, were proposed as mentioned previously.

The earlier study suggested that ATPw is able to reflect different signals between malignant tumors and peritumoral edema, as well as high-grade and low-grade gliomas[84, 85]. These investigations result from that APT has different change rates of cellular proteins in the tumors from the normal contralateral side of the brain[86, 87]. Also, it has been suggested that APTw signals is hypointense in necrotic lesion of tumor regions while the actively growing parts should be isointense. For example, we can conclude that the lower signal intensities inside the active tumor region are the necrosis for the radiation[88]. These characters that being sensitive to mobile protein changes in tumor after radiation prove that APTw signals can provide predicable information and reliable assessments on tumor post-radiation treatments.

In recent study of clinicians, they state that the more standardized and widely available volumetric MR imaging data not only bring them detailed information on tumor detection and treatment assessment, but also emerge an approach to incorporate volumetric measurements[89]. Since the tumors did not undergo pathologic analysis, the ultimately accuracy of the investigation for the ROI on APTw map is suspended. However, in the procedure of

semi-automatic method, the low inter-observer variability reflects a close agreement between different experts. Regarding the manual results, we concluded from this that the accuracy of the semi-automatic method is not inferior to that of the experts. The semi-automatic method matches the expert opinion of the ROI extractions. As stated earlier, manual segmentation is time-consuming and inter-rater variability is considerably high. Therefore, the automatic or semiautomatic methods for tumor ROI extraction will be potentially developed after validated and standardized which have been studied in other organs with promising results[90]. There is much literature on automatic brain tumor segmentation based on T_1w or T_2w[91, 92], especially the widely used voxel-based fuzzy clustering methods[93, 94]. In case of APTw maps, the fusion can cause minor clusters since the change of topology. Similar with Chow et al.[95] method, semi-automatic method relies on the human interface at first step of ROI editing to define the initial mask by roughly drawing the contour of the enclosed tumor. This is the only step rely on the radiologists interactions. The semi-automatic process is considerably faster than manual method (1 min vs. 5 min) in time consumption, which certainly depends on the experience of the radiologists. Importantly, intra-rater reliability was excellent on semi-automatic method by demonstration of good convergent validity, but test-retest reliability over interval of 10 days was lower than optimal using manual desirable. This is because during the editing process, manual method can hardly match an associated contour of the tumor region. An alternative approach on reducing the inter-rater variability was proposed[89], however, the limitation on treatment-induced changes on ROI decision in this study is unavoidable. For our time-dependent MRI multiparameter collection, we are able to be much easier to reach a similar conclusion of contour for uniform subject with highly consistent reproducibility by means of semi-automatic method.

The inter-rater reliability study for two methods revealed that semi-automatic method would be more homogeneous in contrast to the manual method. This criteria based method will help the radiologists to reach a stable result of the ROI extraction. Correct ROI decision is important. It is not only because of the volume estimation *in vivo* for investigating tumor treatments, but also crucial for perfusion, diffusion and other MRI parameters calculation based on ROI. Further exploration on standardization of margin decision of fusion areas is highly desirable on ROI segmentation.

It has been widely believe that ADC values associate with the treatment effects by analyzing tumor grading and differentiation in the past two decades[96, 97]. It is a rough measure of the magnitude of diffusion, including the cell density reduction and water mobility. In pathological process, the increased ADC values relative to normal brain tissue may be affected by tumor growth, edema and necrosis. In the irradiated subject assessment, most of the studies have reported higher ADC values occurred since the apoptotic and/or necrosis processes. Figure 4.5 shows that ADC values have a durable right shift during the tumor development after radiation therapy, except day 4 remained a consistent result as at day 1. Our results of ADC change agreed with previous research[52]. Moreover, in some cases of the unchanged or lower values in ADC signals, the radiation-induced effects, including gliosis, fibrosis, macrophage invasion, vascular changes and demyelization, may be the possible explanation.

ASL technique has been used in quantifying tumor blood flow. Figure 4.2, 4.3 have shown that for both tumor region and the contralateral normal brain tissue, blood flow signals simultaneously decreased in average on ROI during all time of the post-radiation stages. In the meantime, we can detect from Figure 4.4 that after radiation therapy, the tumor parts have an

enhanced contrast with respect to contralateral side. However, in the research of X Hong et al.[52], the reduction of blood flow signals also happened in non-treated rats. This might be attributable to the high intracranial pressure due to the large tumor in the later stage of tumor growth while further investigation is desirable. The DSC MRI technique has shorter scan times and with lower standard deviations than ASL method[98]. However, ASL MRI is non-invasive and also clearly differentiate recurrent tumor and radiation necrosis in patients with gliomas[99, 100]. This is particularly meaningful in clinical treatment for patients since ASL MRI as well as APT use endogenous contrast agents and avoid intravenous injection which is potentially problematic for pediatric cases. Compared with diffusion ADC maps, APT and perfusion blood flow have lower signal-to-noise ratios. Thus, combining the information of perfusion, diffusion and APT, with the conventional imaging method, will likely provide a more detailed and accurate response as a whole picture to be analyzed in clinical treatments. More insightful research on these topics along with standardized criteria is needed in the future.

There are a few limitations in our study. First, we didn't set non-irradiated rat group as our control to compare the tumor development in different period. Second, the number of rats in the experiment was relative small. Third, we didn't follow the survival rate after last time MR imaging collection. Therefore, we could not further decide how the treatment efficiency of low dose radiation (8 Gy) although it is already known that the dose and exposure time for the radiation effects is critical[101, 102]. Finally, our ROI extraction on tumor location is evaluated by ROI area that depends on experts editing while the objective position of the tumor should be analysis by pathology. However, for the *in vivo* situation, the pathology process can cause cerebral injury then the post-stage analysis will be not accurate. In the cases that the rats could

enroll in the histology study, there still might be bias in the position decision of the tumor due to postsurgical changes.

5.2 Thesis contribution

There are several contributions made in our study. First and foremost, multi-parametric MRI biomarkers including T_1, T_2, ADC, blood flow and APTw, have been considered. In order to collect more detail information for clinical treatment, choosing a more accurate tool is desirable. In particular, assessment of current treatments response can influence the decision for the future treatments. Therefore, by means of the messages from perfusion and diffusion MRI parameters, more details in the brain development during the post-radiation therapy will be discovered, especially the differentiation between tumor recurrence and treatment caused necrosis. Conventional MRI alone is not adequate for assessment of the treatment response due to a lack of specificity because of these missing details. Thus, it is believable that this supporting information will help clinician to have more accurate judgment on the patients' condition so that proper medical care can be put into action.

In addition, automatic and semi-automatic segmentation have been compared with manual method in the step of region of interest extraction. Manual methods are the common type of ROI extraction. However, the results depend on the experimenters' experience so the extraction contour can hardly overlap among different examiners. Moreover, manual extraction is time-consuming and easy to make mistake because of the artifacts or errors drawing on the contour, then the users need to redo the ROI drawing. Automatic and semi-automatic

segmentation is more convenient. It saves more time and keeps a more stable result than the manual method. However, since the automatic methods are lack of human interaction and the transition parts between the tumor regions and normal brain tissue is blurring, the automatic results is always far from adequate. To avoid the edge detection mistakes, user interactions is implemented. As the initial condition is set, based on the statistical histogram calculation and thresholding decision as well as morphology process, semi-automatic works efficiently and accurately on edge detection. Even if the exact location of the tumor is hard to decide from the pathology analysis, it provides a more stable conclusion among different experimenters.

Last but not least, our study suggests an interactive idea of implementing image segmentation algorithm in MR imaging processing. Although MR imaging parameters is quite helpful for clinician, some blurring information in the images need more clear explanation or detail presentation so as to lead a more accurate investigation. Some other researches on image processing for MRI have been implemented. For the novel APT parameters, further discussion about its detail presentation is suggested. Therefore, our study takes off a pace to take a deep insight of this new MRI parameter. Also, radiation-therapy detection is also a necessary study in the further. The dose of the radiation should set control group to see how much doses is suitable for rats, and then turn to the cases of clinical treatments for patients. Nevertheless, MRI assessment for treatment response should follow the development and give more instruction for different treatment tools.

5.3 Further study

As mentioned previously, MR imaging parameters are able to aid the clinicians in the whole procedure of patients' treatments for monitor. Even though MRI image segmentation is hard, it can excellently distinguish the variety of soft tissue, and brain images are approximately piecewise constant. However, complex textures in other organs such as lung, it is easy to cause image distortions such as motion artifacts or bias field thanks to the air inside. Also, the structures of interest including tumor, temporal lobes, all have complex shapes. The labels we wish to assign to the objects are usually few and fixed in advance, which are also usually form coherent continuous shapes. One labeled pixel has a high chance to have same mark with its neighbors. Noise is likely to exist in the position of boundaries among different regions. This is also the challenge for the image segmentation in the MRI parameters. Therefore, in the future study, de-noising during or after image segmentation becomes significant factor for the final ROI extraction results. In addition, image processing for not only brain tumor detection, but also other organs of the human body are also desirable. These require deeper insight of different properties.

5.4 Summary

In this thesis, we collected the conventional, perfusion, diffusion and APT MRI parameters during different period of the preradiation and postradiation therapy for thirteen rats. Then it was able to demonstrate that APT and other advanced MRI sequences could provide more details for clinical analysis about treatment assessment, or even being helpful to

differentiate tumor recurrence from treatments caused necrosis. In the step of ROI extraction, semi-automatic method has been proposed and it is more effective and collects stable results from different experimenters. We believe our work in this thesis can reflect the truth that detail information from different MRI sequences can be further investigated along with the image segmentation based semi-automatic method, clinicians' judgments for patients' future treatment plans can be more effective and accurate.

BIBLIOGRAPHY

1. Legler JM, Ries LA, Smith MA, et al. Cancer surveillance series [corrected]: brain and other central nervous system cancers: recent trends in incidence and mortality. *J Natl Cancer Inst.* 1999; 91: 1382-90.
2. Wen PY, Kesari S. Malignant gliomas in adults. *N Engl J Med.* 2008; 359: 492-507.
3. Youland RS, Schomas DA, Brown PD, et al. Changes in presentation, treatment, and outcomes of adult low-grade gliomas over the past fifty years. *Neuro Oncol.* 2013; 15: 1102-10.
4. Garside R, Pitt M, Anderson R, et al. The effectiveness and cost-effectiveness of carmustine implants and temozolomide for the treatment of newly diagnosed high-grade glioma: a systematic review and economic evaluation. *Health Technol Assess.* 2007; 11: iii-iv, ix-221.
5. Nieder C, Adam M, Molls M, et al. Therapeutic options for recurrent high-grade glioma in adult patients: recent advances. *Crit Rev Oncol Hematol.* 2006; 60: 181-93.
6. Canyilmaz E, Uslu GD, Colak F, et al. Comparison of dose distributions hippocampus in high grade gliomas irradiation with linac-based imrt and volumetric arc therapy: a dosimetric study. *Springerplus.* 2015; 4: 114.
7. Tanaka M, Ino Y, Nakagawa K, et al. High-dose conformal radiotherapy for supratentorial malignant glioma: a historical comparison. *Lancet Oncol.* 2005; 6: 953-60.
8. Salazar OM, Rubin P, Feldstein ML, et al. High-Dose Radiation-Therapy in the Treatment of Malignant Gliomas - Final Report. *International Journal of Radiation Oncology Biology Physics.* 1979; 5: 1733-1740.
9. Nakagawa K, Aoki Y, Fujimaki T, et al. High-dose conformal radiotherapy influenced the pattern of failure but did not improve survival in glioblastoma multiforme. *Int J Radiat Oncol Biol Phys.* 1998; 40: 1141-9.
10. Gaspar LE, Fisher BJ, Macdonald DR, et al. Supratentorial malignant glioma: patterns of recurrence and implications for external beam local treatment. *Int J Radiat Oncol Biol Phys.* 1992; 24: 55-7.
11. Liang BC, Thornton AF, Jr., Sandler HM, et al. Malignant astrocytomas: focal tumor recurrence after focal external beam radiation therapy. *J Neurosurg.* 1991; 75: 559-63.
12. Hochberg FH, Pruitt A. Assumptions in the Radiotherapy of Glioblastoma. *Neurology.* 1980; 30: 907-911.
13. Chen W. Clinical applications of PET in brain tumors. *J Nucl Med.* 2007; 48: 1468-81.
14. Verma R, Zacharaki EI, Ou Y, et al. Multiparametric tissue characterization of brain neoplasms and their recurrence using pattern classification of MR images. *Academic Radiology.* 2008; 15: 966-977.
15. Heiss WD, Raab P, Lanfermann H. Multimodality Assessment of Brain Tumors and Tumor Recurrence. *Journal of Nuclear Medicine.* 2011; 52: 1585-1600.
16. Kandpal H, Sharma R, Madhusudhan KS, et al. Respiratory-triggered versus breath-hold diffusion-weighted MRI of liver lesions: comparison of image quality and apparent diffusion coefficient values. *AJR Am J Roentgenol.* 2009; 192: 915-22.
17. Ray N, Acton ST, Altes T, et al. Merging parametric active contours within homogeneous image regions for MRI-based lung segmentation. *Ieee Transactions on Medical Imaging.* 2003;

22: 189-199.
18. Bernick C, Kuller L, Dulberg C, et al. Silent MRI infarcts and the risk of future stroke - The cardiovascular health study. *Neurology.* 2001; 57: 1222-1229.
19. Vlaardingerbroek MT, Boer JA. *Magnetic resonance imaging: theory and practice*, Springer Science & Business Media, 2003.
20. Wright GA. Magnetic resonance imaging. *Ieee Signal Processing Magazine.* 1997; 14: 56-66.
21. Eyster EF, Nielsen SL, Sheline GE, et al. Cerebral radiation necrosis simulating a brain tumor. Case report. *J Neurosurg.* 1974; 40: 267-71.
22. Brandsma D, Stalpers L, Taal W, et al. Clinical features, mechanisms, and management of pseudoprogression in malignant gliomas. *Lancet Oncol.* 2008; 9: 453-61.
23. Brandsma D, van den Bent MJ. Pseudoprogression and pseudoresponse in the treatment of gliomas. *Curr Opin Neurol.* 2009; 22: 633-8.
24. Hicklin DJ, Ellis LM. Role of the vascular endothelial growth factor pathway in tumor growth and angiogenesis. *J Clin Oncol.* 2005; 23: 1011-27.
25. Hasso A, Kortman K, Bradley W. Supratentorial neoplasms. *Magnetic resonance imaging.* 1992; 1: 770-817.
26. Hicks R, Edelman R, Hesselink J, et al. Supratentorial brain tumors. *Clinical magnetic resonance imaging.* 1996; 1: 533-556.
27. Yamasaki F, Kurisu K, Satoh K, et al. Apparent diffusion coefficient of human brain tumors at MR imaging. *Radiology.* 2005; 235: 985-91.
28. Maier SE, Bogner P, Bajzik G, et al. Normal brain and brain tumor: multicomponent apparent diffusion coefficient line scan imaging. *Radiology.* 2001; 219: 842-9.
29. Kono K, Inoue Y, Nakayama K, et al. The role of diffusion-weighted imaging in patients with brain tumors. *AJNR Am J Neuroradiol.* 2001; 22: 1081-8.
30. Taylor DG, Bushell MC. The spatial mapping of translational diffusion coefficients by the NMR imaging technique. *Phys Med Biol.* 1985; 30: 345-9.
31. Ostergaard L, Hochberg FH, Rabinov JD, et al. Early changes measured by magnetic resonance imaging in cerebral blood flow, blood volume, and blood-brain barrier permeability following dexamethasone treatment in patients with brain tumors. *J Neurosurg.* 1999; 90: 300-5.
32. Covarrubias DJ, Rosen BR, Lev MH. Dynamic magnetic resonance perfusion imaging of brain tumors. *Oncologist.* 2004; 9: 528-37.
33. Senger DR, Galli SJ, Dvorak AM, et al. Tumor cells secrete a vascular permeability factor that promotes accumulation of ascites fluid. *Science.* 1983; 219: 983-5.
34. Matsunaga S, Shuto T, Takase H, et al. Semiquantitative Analysis Using Thallium-201 SPECT for Differential Diagnosis Between Tumor Recurrence and Radiation Necrosis After Gamma Knife Surgery for Malignant Brain Tumors. *International Journal of Radiation Oncology Biology Physics.* 2013; 85: 47-52.
35. Buchpiguel CA, Alavi JB, Alavi A, et al. Pet Versus Spect in Distinguishing Radiation Necrosis from Tumor Recurrence in the Brain. *Journal of Nuclear Medicine.* 1995; 36: 159-164.
36. Wen PY, Macdonald DR, Reardon DA, et al. Updated response assessment criteria for high-grade gliomas: response assessment in neuro-oncology working group. *J Clin Oncol.* 2010; 28: 1963-72.

37. Macdonald DR, Cascino TL, Schold SC, Jr., et al. Response criteria for phase II studies of supratentorial malignant glioma. *J Clin Oncol.* 1990; 8: 1277-80.
38. DeLorenzo C, Kumar JS, Zanderigo F, et al. Modeling considerations for in vivo quantification of the dopamine transporter using [(11)C]PE2I and positron emission tomography. *J Cereb Blood Flow Metab.* 2009; 29: 1332-45.
39. Hirvonen J, Johansson J, Teras M, et al. Measurement of striatal and extrastriatal dopamine transporter binding with high-resolution PET and [11C]PE2I: quantitative modeling and test-retest reproducibility. *J Cereb Blood Flow Metab.* 2008; 28: 1059-69.
40. Wintermark M, Sesay M, Barbier E, et al. Comparative overview of brain perfusion imaging techniques. *Stroke.* 2005; 36: e83-99.
41. Feinberg DA, Moeller S, Smith SM, et al. Multiplexed Echo Planar Imaging for Sub-Second Whole Brain FMRI and Fast Diffusion Imaging. *Plos One.* 2010; 5.
42. Forsen S, Hoffman RA. Study of Moderately Rapid Chemical Exchange Reactions by Means of Nuclear Magnetic Double Resonance. *Journal of Chemical Physics.* 1963; 39: 2892-&.
43. Zhou JY, van Zijl PCM. Chemical exchange saturation transfer imaging and spectroscopy. *Progress in Nuclear Magnetic Resonance Spectroscopy.* 2006; 48: 109-136.
44. Aime S, Crich SG, Gianolio E, et al. High sensitivity lanthanide(III) based probes for MR-medical imaging. *Coordination Chemistry Reviews.* 2006; 250: 1562-1579.
45. Sherry AD, Woods M. Chemical exchange saturation transfer contrast agents for magnetic resonance imaging. *Annual Review of Biomedical Engineering.* 2008; 10: 391-411.
46. Zhou JY, Payen JF, Wilson DA, et al. Using the amide proton signals of intracellular proteins and peptides to detect pH effects in MRI. *Nature Medicine.* 2003; 9: 1085-1090.
47. Englande.Sw, Downer NW, Teitelba.H. Hydrogen-Exchange. *Annual Review of Biochemistry.* 1972; 41: 903-&.
48. Wolff SD, Balaban RS. Magnetization transfer contrast (MTC) and tissue water proton relaxation in vivo. *Magn Reson Med.* 1989; 10: 135-44.
49. Zhou JY, Lal B, Wilson DA, et al. Amide proton transfer (APT) contrast for imaging of brain tumors. *Magnetic Resonance in Medicine.* 2003; 50: 1120-1126.
50. Jones CK, Schlosser MJ, van Zijl PCM, et al. Amide proton transfer imaging of human brain tumors at 3T. *Magnetic Resonance in Medicine.* 2006; 56: 585-592.
51. Wen ZB, Hu SG, Huang FH, et al. MR imaging of high-grade brain tumors using endogenous protein and peptide-based contrast. *Neuroimage.* 2010; 51: 616-622.
52. Hong XH, Liu L, Wang MY, et al. Quantitative multiparametric MRI assessment of glioma response to radiotherapy in a rat model. *Neuro-Oncology.* 2014; 16: 856-867.
53. Ho S, Bullitt E, Gerig G. Level-set evolution with region competition: Automatic 3-D segmentation of brain tumors. *16th International Conference on Pattern Recognition, Vol I, Proceedings.* 2002: 532-535.
54. Kaus MR, Warfield SK, Nabavi A, et al. Automated segmentation of MR images of brain tumors. *Radiology.* 2001; 218: 586-591.
55. Badran EF, Mahmoud EG, Hamdy N. An Algorithm for Detecting Brain Tumors in MRI Images. *Icces'2010: The 2010 International Conference on Computer Engineering & Systems.* 2010: 368-373.
56. Tang H, Wu EX, Ma QY, et al. MRI brain image segmentation by multi-resolution edge detection and region selection. *Computerized Medical Imaging and Graphics*. 2000; 24:

349-357.

57. A wavelet-based approach to detect bladder tumor in color images. *TENCON 99. Proceedings of the IEEE Region 10 Conference*. IEEE, 1999.
58. Wang JZ, Kong J, Lu YH, et al. A modified FCM algorithm for MRI brain image segmentation using both local and non-local spatial constraints. *Computerized Medical Imaging and Graphics.* 2008; 32: 685-698.
59. Heindel WC, Jernigan TL, Archibald SL, et al. The relationship of quantitative brain magnetic resonance imaging measures to neuropathologic indexes of human immunodeficiency virus infection. *Arch Neurol.* 1994; 51: 1129-35.
60. Guttmann CR, Jolesz FA, Kikinis R, et al. White matter changes with normal aging. *Neurology.* 1998; 50: 972-8.
61. Li C, Huang R, Ding Z, et al. A level set method for image segmentation in the presence of intensity inhomogeneities with application to MRI. *IEEE Trans Image Process.* 2011; 20: 2007-16.
62. Lin KCR, Yang MS, Liu HC, et al. Generalized Kohonen's competitive learning algorithms for ophthalmological MR image segmentation. *Magnetic Resonance Imaging.* 2003; 21: 863-870.
63. Akay B. A study on particle swarm optimization and artificial bee colony algorithms for multilevel thresholding. *Applied Soft Computing.* 2013; 13: 3066-3091.
64. Pal NR, Pal SK. A Review on Image Segmentation Techniques. *Pattern Recognition.* 1993; 26: 1277-1294.
65. Prastawa M, Bullitt E, Ho S, et al. A brain tumor segmentation framework based on outlier detection. *Medical Image Analysis.* 2004; 8: 275-283.
66. Bullitt E, Gerig G, Pizer SM, et al. Measuring tortuosity of the intracerebral vasculature from MRA images. *IEEE Trans Med Imaging.* 2003; 22: 1163-71.
67. Lin W, An H, Chen Y, et al. Practical consideration for 3T imaging. *Magn Reson Imaging Clin N Am.* 2003; 11: 615-39, vi.
68. Osher S, Sethian JA. Fronts Propagating with Curvature-Dependent Speed - Algorithms Based on Hamilton-Jacobi Formulations. *J Comput Phys.* 1988; 79: 12-49.
69. Stuart A, Ord JK. Kendall's Advanced Theory of Statistics, Volume I: Distribution Theory. *Arnold, London.* 1994.
70. Kass M, Witkin A, Terzopoulos D. Snakes - Active Contour Models. *International Journal of Computer Vision.* 1987; 1: 321-331.
71. Raviv TR, Gao Y, Levitt JJ, et al. Statistical Shape Analysis of Neuroanatomical Structures via Level-Set-based Shape Morphing. *Siam Journal on Imaging Sciences.* 2014; 7: 1645-1668.
72. Sezan MI. A peak detection algorithm and its application to histogram-based image data reduction. *Computer vision, graphics, and image processing.* 1990; 49: 36-51.
73. Otsu N. A threshold selection method from gray-level histograms. *Automatica.* 1975; 11: 23-27.
74. Pun T. A New Method for Grey-Level Picture Thresholding Using the Entropy of the Histogram. *Signal Process.* 1980; 2: 223-237.
75. Kapur JN, Sahoo PK, Wong AKC. A New Method for Gray-Level Picture Thresholding Using the Entropy of the Histogram. *Computer Vision Graphics and Image Processing.* 1985; 29: 273-285.
76. Chang CI, Chen K, Wang JW, et al. A Relative Entropy-Based Approach to Image

Thresholding. *Pattern Recognition.* 1994; 27: 1275-1289.

77. Luthon F, Lievin M, Faux F. On the use of entropy power for threshold selection. *Signal Process*. 2004; 84: 1789-1804.
78. Odland A, Server A, Saxhaug C, et al. Volumetric glioma quantification: comparison of manual and semi-automatic tumor segmentation for the quantification of tumor growth. *Acta Radiol*. 2014.
79. Chang CI, Du Y, Wang J, et al. Survey and comparative analysis of entropy and relative entropy thresholding techniques. *Iee Proceedings-Vision Image and Signal Processing.* 2006; 153: 837-850.
80. Bland JM, Altman DG. Statistical Methods for Assessing Agreement between Two Methods of Clinical Measurement. *Lancet.* 1986; 1: 307-310.
81. Hayen A, Dennis RJ, Finch CF. Determining the intra- and inter-observer reliability of screening tools used in sports injury research. *Journal of Science and Medicine in Sport.* 2007; 10: 201-210.
82. Gajdosik RL, Bohannon RW. Clinical measurement of range of motion. Review of goniometry emphasizing reliability and validity. *Phys Ther.* 1987; 67: 1867-72.
83. Downing SM. Reliability: on the reproducibility of assessment data. *Med Educ.* 2004; 38: 1006-12.
84. Zhou JY, Blakeley JO, Hua J, et al. Practical data acquisition method for human brain tumor amide proton transfer (APT) imaging. *Magnetic Resonance in Medicine.* 2008; 60: 842-849.
85. Zhou JY, Zhu H, Lim M, et al. Three-Dimensional Amide Proton Transfer MR Imaging of Gliomas: Initial Experience and Comparison With Gadolinium Enhancement. *Journal of Magnetic Resonance Imaging.* 2013; 38: 1119-1128.
86. Hobbs SK, Shi G, Homer R, et al. Magnetic resonance image-guided proteomics of human glioblastoma multiforme. *J Magn Reson Imaging.* 2003; 18: 530-6.
87. Howe FA, Barton SJ, Cudlip SA, et al. Metabolic profiles of human brain tumors using quantitative in vivo H-1 magnetic resonance spectroscopy. *Magnetic Resonance in Medicine.* 2003; 49: 223-232.
88. Wang SL, Tryggestad E, Zhou TT, et al. Assessment of MRI Parameters as Imaging Biomarkers for Radiation Necrosis in the Rat Brain. *International Journal of Radiation Oncology Biology Physics.* 2012; 83: E431-E436.
89. Sorensen AG, Batchelor TT, Wen P, et al. Response criteria for glioma. *Nature Clinical Practice Oncology.* 2008; 5: 634-644.
90. Mozley PD, Bendtsen C, Zhao BS, et al. Measurement of Tumor Volumes Improves RECIST-Based Response Assessments in Advanced Lung Cancer. *Translational Oncology.* 2012; 5: 19-25.
91. Balafar MA, Ramli AR, Saripan MI, et al. Review of brain MRI image segmentation methods. *Artificial Intelligence Review.* 2010; 33: 261-274.
92. Llado X, Oliver A, Cabezas M, et al. Segmentation of multiple sclerosis lesions in brain MRI: A review of automated approaches. *Information Sciences.* 2012; 186: 164-185.
93. Vaidyanathan M, Clarke LP, Hall LO, et al. Monitoring brain tumor response to therapy using MRI segmentation. *Magnetic Resonance Imaging.* 1997; 15: 323-334.
94. Corso JJ, Sharon E, Dube S, et al. Efficient multilevel brain tumor segmentation with integrated Bayesian model classification. *Ieee Transactions on Medical Imaging.* 2008; 27:

629-640.

95. Chow DS, Qi J, Guo X, et al. Semiautomated Volumetric Measurement on Postcontrast MR Imaging for Analysis of Recurrent and Residual Disease in Glioblastoma Multiforme. *American Journal of Neuroradiology.* 2014; 35: 498-503.

96. Bulakbasi N, Kocaoglu M, Ors F, et al. Combination of single-voxel proton MR spectroscopy and apparent diffusion coefficient calculation in the evaluation of common brain tumors. *American Journal of Neuroradiology.* 2003; 24: 225-233.

97. Bulakbasi N, Guvenc I, Onguru O, et al. The added value of the apparent diffusion coefficient calculation to magnetic resonance imaging in the differentiation and grading of malignant brain tumors. *J Comput Assist Tomogr.* 2004; 28: 735-46.

98. Essig M, Shiroishi MS, Nguyen TB, et al. Perfusion MRI: The Five Most Frequently Asked Technical Questions. *American Journal of Roentgenology.* 2013; 200: 24-34.

99. Law M, Young RJ, Babb JS, et al. Gliomas: Predicting time to progression or survival with cerebral blood volume measurements at dynamic susceptibility-weighted contrast-enhanced perfusion MR imaging. *Radiology.* 2008; 247: 490-498.

100. Hu LS, Eschbacher JM, Heiserman JE, et al. Reevaluating the imaging definition of tumor progression: perfusion MRI quantifies recurrent glioblastoma tumor fraction, pseudoprogression, and radiation necrosis to predict survival. *Neuro-Oncology.* 2012; 14: 919-930.

101. Walker MD, Strike TA, Sheline GE. An analysis of dose-effect relationship in the radiotherapy of malignant gliomas. *Int J Radiat Oncol Biol Phys.* 1979; 5: 1725-31.

102. Merchant TE, Hua CH, Shukla H, et al. Proton versus photon radiotherapy for common pediatric brain tumors: comparison of models of dose characteristics and their relationship to cognitive function. *Pediatr Blood Cancer.* 2008; 51: 110-7.

CURRICULUM VITAE

EDUCATION

Johns Hopkins University Baltimore, MD

Master of Biomedical Engineering and Computer Science May 2015

- Laboratory: Radiology Laboratory & Center of Imaging Science
- Teaching Assistant to Undergraduate
- Recipient of Full Merit Scholarship

Tianjin University Tianjin, China

Bachelor of Engineering, Computer Science and Technology June 2012

- Laboratory: Computer Vision
- National Scholarship Recipient from 2008 to 2010
- Graduated First in Class

Tohoku University Sendai, Japan

Exchange Program, School of Computer Engineering August 2010

- Laboratory: Aoki Laboratory of Imaging
- National Scholarship Recipient from 2010 to 2011

INDUSTRY EXPERIENCE

Hisense Hi-Tech Corporation Qingdao, China

R&D Project Lead April 2012 – May 2013

- Developed and implemented support plans of new product to ensure successful launch
- Led programs including customer testimonials and product demonstrations in support of product launches
- Served as the point person for all troubleshooting and customer communication in the assigned Qingdao area
- Analyzed algorithms and collected data to update projects according to research requirements
- Led and worked with a team of 12 in R & D department, using OpenCV library and built up Electronic Police in MFC project
- Worked independently on implementing signal lights identification for enforcing the traffic rules

RESEARCH EXPERIENCE

Image Segmentation on Region of Interest Baltimore, MD

Advisor: Professor Jinyuan Zhou October 2014 – present

- Apply and develop proper algorithm with MATLAB and C++ by implement level set method and threshold detection to extract Region of Interest for Magnetic Resonance Imaging results. Studying mouse brains with tumor as objects, to prove Amide Proton Transfer (APT) imaging method is more efficient than usual ones, we need to prove it can detect tumor region more accurate than other imaging methods.

Mouse Brain Learning Baltimore, MD

Advisor: Professor Michael I. Miller September 2013 – September 2014

- Studied the process of analyzing data in the mouse brain. Preprocess the atlas and the subjects, to gain region of interest. Then use LDDMM algorithm to gain quality control, leading to the results of grayscale and binary ROIs. The phase difference between two input fingerprints from database (obtain the information from space domain to frequency domain base on Fourier transfer theory)

Fingerprint Matching using POC (Phase-Only Correlation) Sendai, Japan

Advisor: Professor Takafumi Aoki December 2010 – July 2011

- Study the phase difference between two input fingerprints from database (obtain the information from space domain to frequency domain base on Fourier transfer theory)
- Analyzed equal error rate to evaluate the performance of the proposed algorithm

Image Segmentation and Application on DepthMap Recovering Tianjin, China

Advisor: Professor ShiguangLiu

- Studied the Image Segmentation algorithms (learning K-means and Energy-Minimization Function to take into use)
- Analyzed the depthmap calculation process and make use of it in segmentation to improve the effect of result

ADDITIONAL INFORMATION

- Computer Skills: C&C++, Visual Studio, Java, Linux, Microsoft Office, Photoshop, MATLAB, OpenCV, Auto-CAD, LATEX
- Publication: “Assessment of Glioma Response to 8 Gy Radiotherapy on Multiple MRI Biomarkers by Applying Image Segmentation Algorithm”
- Volunteer Activities: Volunteered in Sichuan School District after Earthquake (2012), part of the foreign volunteers in Japan after the 311 Earthquake in 2011, environmental protection project “Against the Pollution” (2009)
- Languages: Fluent in English and Mandarin Chinese
- Interests: Tennis, Volunteer Work, etc.